



Geochemical, isotopic, and fluid inclusion signatures of Zn-Pb mineralization in the Tiran mining district, Isfahan, Sanandaj-Sirjan zone (Iran)



Mostafa Nejadhadad^a, Batoul Taghipour^{a,*}, David R. Lentz^b

^a Department of Earth Sciences, College of Sciences, Shiraz University, Shiraz, Iran

^b Department of Earth Sciences, University of New Brunswick, Fredericton, NB E3B 5A3, Canada

ARTICLE INFO

Keywords:

Fluid mixing
Sulfur isotopes
Lead isotopes
Fault-controlled Zn-Pb mineralization
Tiran mining district

ABSTRACT

In Tiran base-metal district, the post-Early Cretaceous epigenetic Zn-Pb deposits occur as fault-controlled pocket-like lenses. The main structural feature of mineralization is its association with a district-scale strike-slip fault, which cuts an en-echelon folded terrane. Mineralization occurs as sphalerite, galena, pyrite, and minor chalcopyrite found within massive ore, breccia textures, veins and veinlets, disseminated grains and carbonate replacements along tectonized limestone-shale contacts. The cumulative reserves of this district is 10 Mt grading at 6% Zn + Pb. Host rock silicification and calcitization formed during hydrothermal alteration. Fluid inclusion data revealed that ore minerals precipitated due to the mixing of two fluids, one determined from sphalerite-hosted inclusions (Homogenization temperature: 155 °C and salinity: 19 wt% NaCl_{equiv.}) and the other observed in quartz inclusions (Th: 184.5 °C and salinity: 12.5 wt% NaCl_{equiv.}). The sulfur isotope compositions of sulfide minerals vary between −8.92 and +4.15‰ and ranged from 22.61 to 23.88‰ for barite, thus suggesting an Early Tertiary marine sulfate influence. Sulfur isotopic data favor two sources of sulfur: bacteriogenic activity ($\delta^{34}\text{S}_{\text{CDT}}$ −9 to −6‰) and thermochemical sulfate reduction ($\delta^{34}\text{S}$: −1 to +4‰). The $^{206}\text{Pb}/^{204}\text{Pb}$, $^{207}\text{Pb}/^{204}\text{Pb}$, and $^{208}\text{Pb}/^{204}\text{Pb}$ ratios (18.1–18.4, 15.6–15.7, and 38.4–38.6, respectively) reflect upper crustal basement rocks as the source of metals. Fertile ore fluids mixed within fault zones, along the contacts of limestone and shale. Base metal deposition during fluid mixing could be a result of increasing reduced sulfur, cooling, and decreasing ligand activity after tectonic movements. The multiple lines of evidence presented here are consistent with the mineralization in the Tiran mining district being similar to Mississippi Valley-type deposits.

1. Introduction

The Isfahan-Malayer Pb-Zn belt has been documented by Ziserman and Momenzadeh (1972), Momenzadeh and Rastad (1973), Förster (1978), and most recently Rajabi et al. (2012). This Cretaceous carbonate platform (McQuarrie et al., 2003; Alavi, 2004; Golonka, 2004; Ghasemi and Talbot, 2006; Seton et al., 2012) is host to more than 250 ore deposits and prospects (Ghorbani, 2013). These deposits are mainly strata-bound and, in most cases, show discordant features with the enclosing strata. They have facies transitions between the shale and carbonate, but have no obvious genetic relation with igneous rocks (Momenzadeh, 1976; Förster, 1974, 1978; Momenzadeh et al., 1979; Rastad et al., 1980; Ghazban et al., 1994; Ehya et al., 2010; Rajabi et al., 2012; Nejadhadad et al., 2016; Hosseini-Dinani and Aftabi, 2016). Previous work has documented the geological and mineralogical

characteristics of some deposits, e.g., Ahangaran (Momenzadeh, 1976; Momenzadeh et al., 1979), Irankuh (Rastad et al., 1980), Ravanj, and Tiran (Rajabi et al., 2012), that favor an initial syngenetic (exhalative) mineralization model. However, other studies including Förster (1974, 1978), Ghazban et al. (1994), Ehya et al. (2010), Nejadhadad et al. (2016), and Hosseini-Dinani and Aftabi (2016) accepted an epigenetic origin (MVT) for this mineralization.

The Tiran district is one of several mining districts along the 600-km length of the Isfahan-Malayer Pb-Zn metallogenic belt, located 50 km north of the city of Isfahan (32°42'N and 53°09'E). The Tiran mining district has been exploited since 1960. Mineralization includes five separated pocket and tabular orebodies (Ckeck Ab, Old Anjireh, Vejin-e-Bala, Vejin-e-Pain, and Tire-Vejin) found within three hills located in the district. Ore reserves total 10 million metric tonnes grading 4% Zn and 2% Pb and 30 ppm Ag. Despite decades of production, the

* Corresponding author.

E-mail address: taghipour@shirazu.ac.ir (B. Taghipour).

<https://doi.org/10.1016/j.oregeorev.2018.08.005>

Received 23 September 2017; Received in revised form 3 June 2018; Accepted 5 August 2018

Available online 06 August 2018

0169-1368/ Crown Copyright © 2018 Published by Elsevier B.V. All rights reserved.

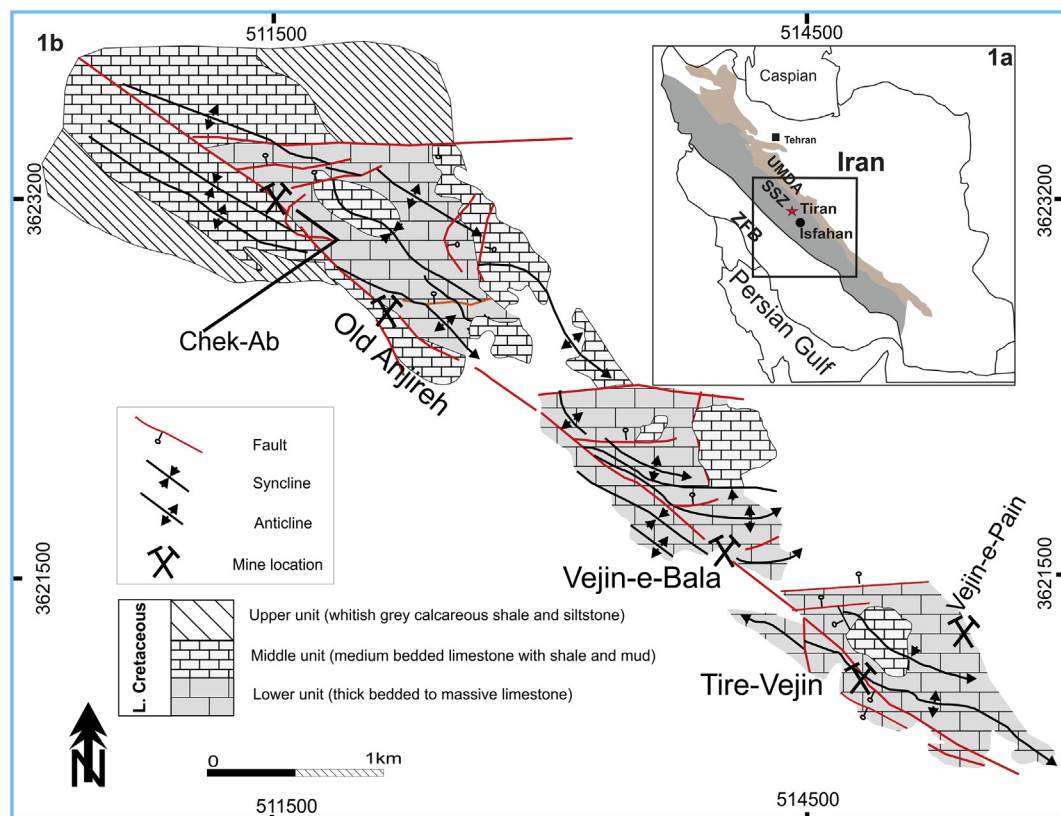


Fig. 1. a) Location of the study area in the Zagros Orogenic Belt within the Sanandaj-Sirjan Zone (SSZ); b) Geological map of the Tiran mining district (modified from Lisenbee and Uzunlar, 1988) including the Check-Ab, Old Anjireh, Vejin-e-Bala, Vejin-e-Pain, and Tire-Vejin orebodies.

geological and geochemical controls on mineralization in the Tiran district remain undocumented. To better address the genesis of the Tiran Zn-Pb deposits, the mineralizing environment is assessed by describing the geological and structural controls, coupled with fluid inclusion, as well as sulfur and lead isotopic analyses.

2. Geology of the study area

The geology of Iran reflects mainly the results of the opening and closure of the Paleo- and Neo-Tethys seas. The Neo-Tethys seafloor was subducted beneath the Iranian Plate, producing the Zagros orogenic belt (Stöcklin, 1968; Jankovic, 1977, 1997; Förster, 1978; Berberian and Berberian, 1981; Mohajjel and Fergusson, 2000; Mohajjel et al., 2003; Ghasemi and Talbot, 2006). The Zagros Orogen has been subdivided into three subzones, from south to north, including: 1) the Zagros Fold-Thrust Belt, a probable continental margin of the Arabian plate, 2) the Sanandaj-Sirjan Magmatic and Metamorphosed Zone (SSZ), a probable Mesozoic fore-arc of the Iranian plate, and 3) the Uromieh-Dokhtar Magmatic Arc (UDMA) (Berberian and King, 1981; Alavi, 1994; Agard et al., 2005; Ghasemi and Talbot, 2006). The Tiran mining district lies in the SSZ (Fig. 1). The rocks of the NW-SE trending SSZ were highly deformed during the Zagros Orogeny (Stöcklin, 1968; Berberian and King, 1981; Hooper et al., 1994; Mohajjel et al., 2003; Agard et al., 2005). Metallogeny of the SSZ is complicated and includes Paleozoic metamorphosed iron deposits, Triassic to Cretaceous shale and carbonates that host Ba-F mineralization, Lower Cretaceous carbonate-hosted Pb-Zn mineralization, Upper Cretaceous iron mineralization related to plutonic rocks, and Eocene gold deposits hosted by metamorphosed rocks (Stöcklin, 1968; Förster, 1974, 1978; Moritz et al., 2006; Verdel, 2009, 2011, 2013; Nabatian et al., 2015).

The study area is part of a large anticlinorium. The Upper Triassic-Jurassic sediments (Shemshak Formation) of the study area are composed of dark grey shale with sandstone intercalations. These strata are

exposed in the core of the anticlinoria, north of the Tiran territory (Seyed Emami et al., 1973). The > 800-m-thick Barmian-Albian sequences (carbonate rocks) overlie the Shemshak shales (Zahedi, 1975). The Cretaceous sequences began with deposition of disconformable terrigenous red sandstone and conglomerate. This type of progressive terrigenous strata was previously reported in the neighboring deposits of the Isfahan-Malayer, e.g., the Irankuh Pb-Zn deposit (Ghazban et al., 1994). Terrigenous strata grade upwards into sandy dolomite for a combined thickness of 50 m. Orbitolina-bearing carbonate beds are up to 10 m-thick and overlie the terrigenous strata. The thick-bedded to massive, resistant limestone is about 500 m-thick. Medium-bedded limestone with shale and mud layers, 200 m thick, overlies the thick-bedded limestone (Fig. 1). A whitish-grey calcareous shale conformably, in turn, overlies the limestone and shale member. Ammonites occur within this member and an Albian age has been proposed for these strata (Seyed Emami et al., 1973) (Fig. 1). The main ore zone occurs in thick to medium-bedded grey orbitolina limestone (Fig. 2), although some minor mineralization occurs in other strata of the Lower Cretaceous sequences. Above the studied sequences, conglomerate, marl, nummulitic limestone, sandy limestone, as well as red sandstone and conglomerates with evaporates comprise much of the Eocene to Pliocene strata.

In the Tiran district, a northwest-trending strike-slip fault marked by multiple movements cuts across the southwest flanks of three hills. Lisenbee and Uzunlar (1988) argued that this fault forms part of wrench fault system based on the dextral movement, compression of the folds near the faults, vertical rotation of the limbs, and the flexural slip. East-trending normal faults down drop the lower limestone unit on the north side of the hills below the alluvial plain. It seems that a north-south extensional phase existed prior to mineralization (Lisenbee and Uzunlar, 1988).

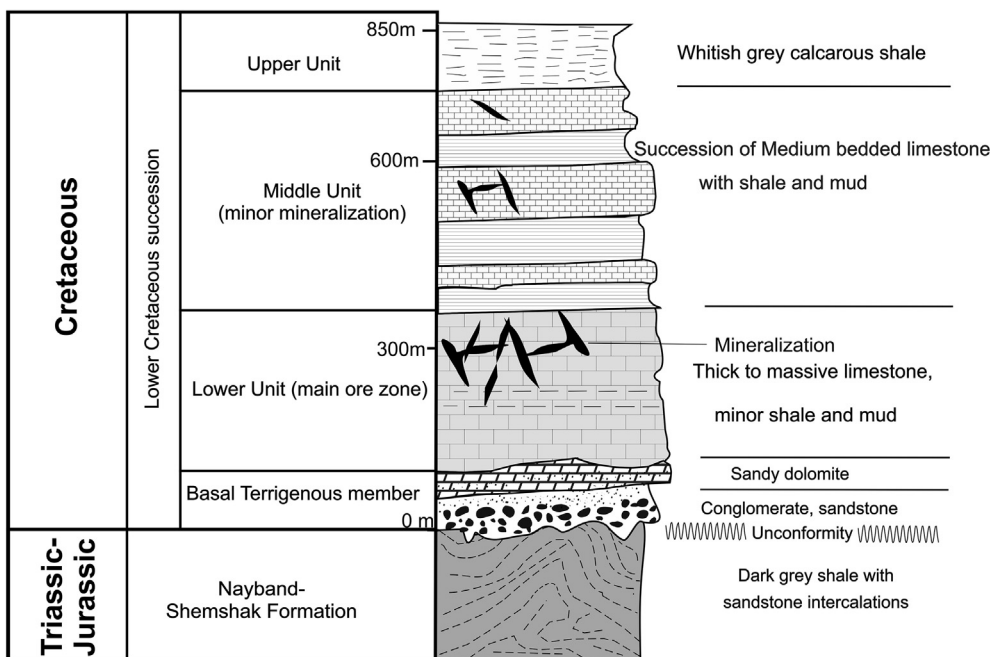


Fig. 2. Stratigraphic column of the Tiran Zn-Pb mining district showing epigenetic vein-type mineralized horizons. Ore shown by dark vein and breccia bodies in the Lower and Middle unit carbonates.

3. Mineralization and geometry of orebodies

3.1. Mineralization

Mineralization in the Tiran district is generally manifested as fine-grained massive ore, brecciated textures containing angular clasts of limestone, small veins, veinlets, medium- to coarse-grained disseminated crystals, and replacement of carbonate-bearing host rocks (Fig. 3). The paragenetic summary of the mineralization, used as the

framework for our subsequent geochemical and fluid inclusion studies, is illustrated in Fig. 4. Framboidal pyrite, presented as fine-grained spherules, is the first sulfide to crystallize, likely deposited with the host rock in a syndiagenetic process. Pre-mineralization calcite and minor dolomite were deposited epigenetically. During the mineralization stage, silicification of the host rock and precipitation of stage 2 pyrite was followed by red to orange sphalerite (I), and minor quantities of tetrahedrite, rare chalcopyrite, galena (I), quartz, yellow sphalerite (II), galena (II), late-idiomorphic coarse-grained pyrite, minor barite, and



Fig. 3. Structural features of the Old Anjireh mineralization in the shale-limestone contact. A) Mineralized limestone slab restricted to shale-rich strata. B, C and D shown selected parts (I, II and III) of A in detail. B) Hydrothermally brecciated limestone filled by sphalerite (Sph), galena (Gn), and calcite (I). C) Stratabound sphalerite-galena ore, replacing limestone (II). D) Sulfide minerals replacing thin bedded limestone intercalated with shale (III).

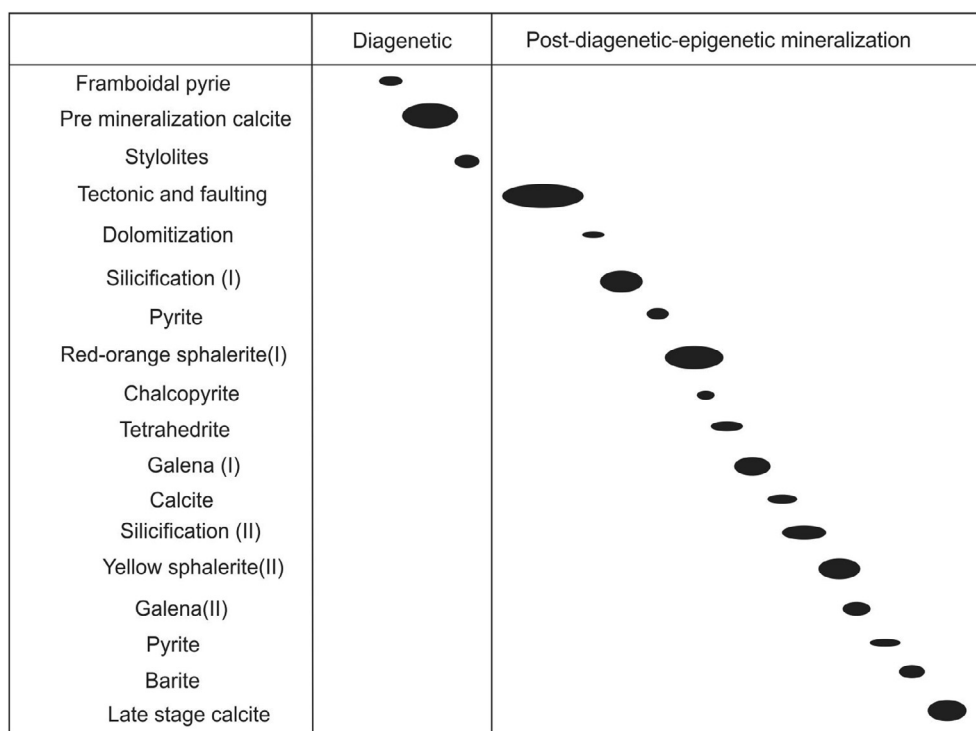


Fig. 4. Paragenetic sequence of ore and alteration mineralogy, Zn-Pb Tiran mining district.

late-stage calcite (Fig. 5a–f).

Red to yellowish Fe-poor sphalerite is the main ore mineral ($Zn/Pb > 2.5$) in Tiran orebodies, except for the Vejin-e-Pain deposit where galena is more common than sphalerite (3–7% Pb in contrast to 1–4% Zn). It is important to note that the relative abundance of sphalerite and galena varies from one orebody to another as well as within individual orebodies. Two stages of sphalerite deposition can be distinguished in Tiran orebodies. The earliest is a fine-grained, red to orange sphalerite (sphalerite I) followed by a later honey-yellow sphalerite (sphalerite II). Red and yellow sphalerite-banded veins alternate with calcite and quartz. Sphalerite grains are ≤ 1 mm in diameter and individual galena grains are ≤ 3 -mm-wide. Locally disseminated sphalerite (I) is present in argillaceous limestone and is ≤ 5 -mm-wide. It appears that sphalerite was deposited during part of the structural development of the rock body (Lisenbee and Uzunlar, 1988). Sphalerite shows calcite pressure shadows and is cut by small veins of calcite. The first deposition of galena occurs after sphalerite I and it belongs to the main stage of ore mineralization. Yellow sphalerite (II) contains inclusion of galena and is also mantled by a layer of galena. Well-crystallized vugs filled with grains of galena imply that growth slowed through the evolution of fluid system (paragenetic sequence). Replacement of the micritic matrix of carbonate rocks by sulfide minerals (sphalerite and galena) was observed in the Vejin-e-Bala and Old Anjireh deposits. Matrix replacement occurs as anhedral fine-grained minerals, approximately 0.3 mm in length (Fig. 5d–f). Aggregates of galena grains have irregular outlines, elongated parallel to the layering. Chalcopyrite crystals are minute grains in galena aggregates. Tetrahedrite is mainly deposited after red sphalerite and before or within main stage galena (galena I). Tetrahedrite is distributed sporadically in ore, engulfing sphalerite inclusions and shows intergrowth textures with main stage galena.

Pyrite, quartz, and calcite are abundant gangue minerals, with dolomite and barite in low abundance. Three stages of pyrite occurrences are recognized. The earliest is framboidal pyrite stemming from bacteriogenic activity (Kucha et al., 2010; Nejadhadad et al., 2016). The bulk of this pyrite deposited in shale, siltstone, and black limestone. The second stage of pyrite formation occurs with the initial precipitation of epigenetic sulfide mineral. These types of pyrite are enclosed and

replaced by other sulfide minerals. The third pyrite stage is deposited as cubic crystals, ranging up to 2 cm in diameter.

Calcite is often deposited as a pre-mineralization mineral and also in a late-stage. Late-stage calcite generally fills open spaces between ore minerals. It is characterized by white and grey anhedral macrocrystals. Minor dolomite deposited after incipient replacement of carbonate host rock by quartz (Fig. 5) was followed by ore mineral replacement and then by a later stage of quartz deposition. Red to orange sphalerite and quartz have overlapping paragenesis, however yellow sphalerite replaced quartz. Banded veins of red-orange sphalerite and quartz provide textural evidence for multiple overlapping pulses (Shadlun, 1982).

3.2. Geometry of orebodies

The geometry and localization of the orebodies in the Tiran district is complex and mainly controlled by both stratigraphic and tectonic features. The main ore zones of the Tiran Zn-Pb deposit are found in the lower limestone unit that lies beneath—or was emplaced via tectonic contact with the shale-rich strata. Minor mineralization also occurs in the shale-rich carbonates of the middle units. In plane view, all orebodies, except for Vejin-e-Pain, lie along the SE-NW regional wrench fault system. The carbonate host rocks of the Chek-Ab, Old Anjireh, Vejin-e-Bala, and Tire-Vejin orebodies are in tectonic contact with impermeable shale-rich layers (Figs. 6a–d and 4a–d). High angle, north-dipping parallel faults of the wrench system consist of intensely deformed carbonate of the mineralized zone. In most cases, strongly fractured limestone and shale have been juxtaposed along faults (Fig. 7). The sulfide orebodies are tabular, lens, or pocket-shaped and are restricted to the lithological boundaries. In the Chek-Ab and Old Anjireh deposits, orebodies have 25–35 m wide; lie in strongly deformed zones between parallel faults of the wrench system. Mineralization occurred in fractures of the lower unit limestone and middle limestone-shale intercalation (Figs. 6 and 7). The strongest mineralization is present at the junction of the wrench fault and the east-trending normal faults (Lisenbee and Uzunlar, 1988). Mineralization in the Old Anjireh system occurred along the wrench fault zone, which extends 450 m long and 40 m high. The Vejin-e-Bala orebody form a

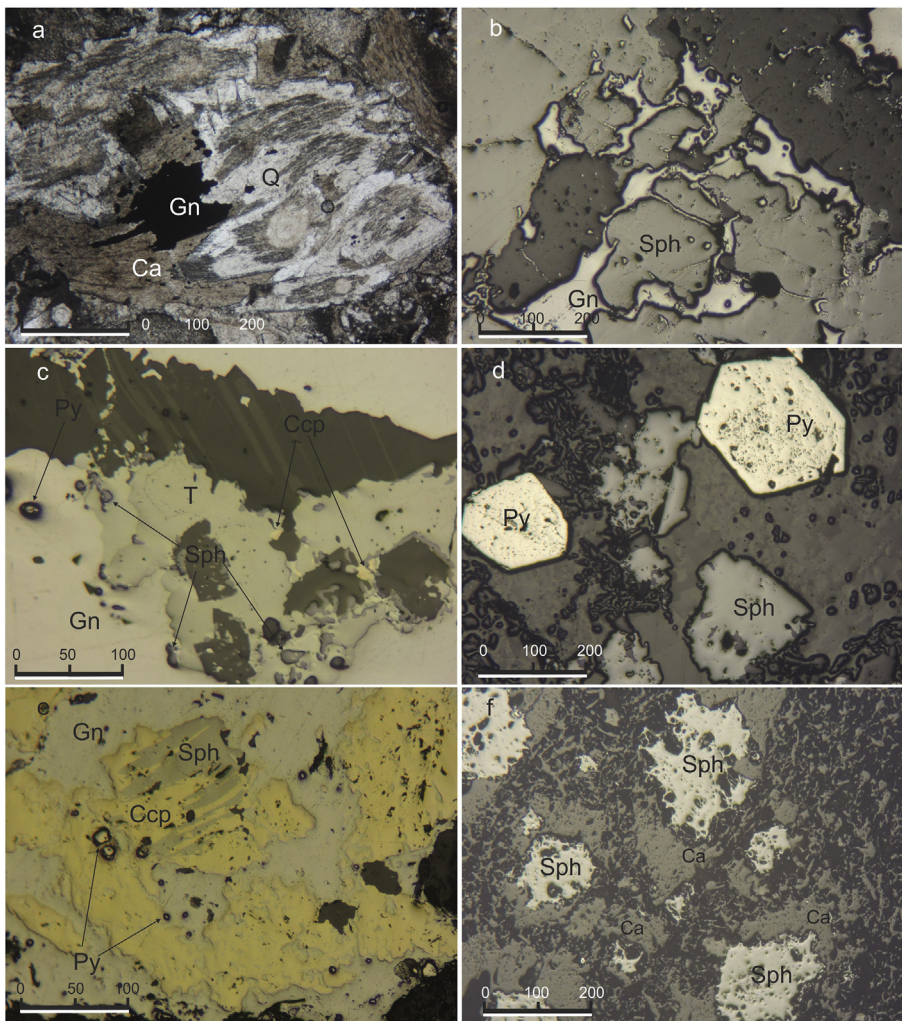


Fig. 5. Photomicrographs of representative textures of ore and gangue minerals in reflected plane polarized light from the Tiran mining district. a) Host rock silicification after sparitization (transmitted PPL), b) Galena deposited in cracks of sphalerite (reflected PPL), c) Pyrite and sphalerite inclusions in galena, tetrahedrite intergrowth with galena (reflected PPL), d) Sphalerite intergrowth with pyrite in silicified carbonate matrix (reflected PPL), e) Pyrite inclusions in both galena and chalcopyrite; sphalerite and chalcopyrite show intergrowth but they are deposited before galena (reflected PPL), f) Sphalerite within recrystallized carbonate (reflected PPL). Q – quartz, Ca – calcite, Sph – sphalerite, Gn – galena, Py – pyrite, Ccp – chalcopyrite.

tabular sheet dipping 50°N, with 800 m length and 10–30 m wide, occurs along the wrench fault. Mineralization is well developed in the lower unit limestone of the hanging wall and to a lesser extent in the middle unit with limestone-shale intercalations. Ore grades vary sharply across the fault zone. Mineralized fault zones are surrounded by non-mineralized weakly crushed/brecciated (cataclastic) rocks. Thus, structural and stratigraphic features are the main controls on mineralization.

In the Vejin-e-Pain deposit, the lithofacies specifically influenced mineralization. Here, the uppermost layers of altered fossiliferous limestone contain disseminated galena and to a lesser extent sphalerite, chalcopyrite, and pyrite. The northeasterly-dipping disseminated mineralization is approximately 30,000 m² with a thickness of 7 m.

4. Materials and methods

To obtain a comprehensive and representative survey of mineral paragenesis, approximately 150 samples were collected from surface outcrops of the Chek-Ab, Old Anjireh, Vejin-e-Pain, and Tire-Vejin ore deposits. Textural studies were conducted on hand specimens using the Dickson carbonate staining of polished samples and petrographic methods (transmitted and reflected light). Inductively Coupled Plasma-Mass Spectrometry (ICP-MS) analyses were performed on eight pure red and yellow sphalerite minerals and six galena samples collected from the different orebodies separated by hand-picking using a binocular microscope; different types of mineralization include breccia fillings, disseminated and vein-type mineralization (Table 1). The samples were

analyzed by ICP-MS after high temperature (105°C), aqua regia acid digestion at LabWest in Australia. The estimated detection limit of elements in sphalerite and galena are Ag (0.01 ppm), As, Sb (0.1 ppm), Cd, Cu (0.2 ppm), Ge, Ga, Co, Ni (1 ppm). Doubly polished sphalerite, quartz, and calcite samples were prepared for fluid inclusion microthermometry measurements. These analyses were made using a Linkam THMS-600 heating and freezing stage at the Iranian Mining Institution Processing Research Center (IMPRC). Calibration was done using cesium nitrate and n-hexane with a precision of ± 0.1 °C below 0 °C and ± 0.6 °C for the homogenization temperature. Salinity of the fluid inclusions was calculated using the experimental data of Bodnar (1993) in wt% NaCl equivalent (Table 2). The criteria of Roedder (1984) were used for petrography and recognition of primary inclusions. Sulfur isotope analysis was done at the University of California Davis stable isotope analysis facility. The sulfur isotopes ($\delta^{34}\text{S}$ values) were measured by an elemental vario isotope cube interfaced to a Ser Con 20-22 IRMS packed with tungsten oxide. Subsequently, sample gases were reduced with elemental copper at 880 °C. Following separation, the sample SO₂ passed directly to the IRMS for measurement. Calibration was done against IAEA S.1, S.2, S.3, IAEA-SO-5, IAEA-SO-6, and HHS standards. The results are reported in per mil (‰) relative to V-CDT. The long-term reproducibility of this method is ± 0.4‰. Lead isotope analyses were performed on four galena and two sphalerite samples of Tiran deposits at the Earth Resources Research and Analysis (TERRA) facility at Memorial University of Newfoundland, Canada (Table 4). Approximately 0.2 g of powder was dissolved in Savilex® teflon beakers using a mixture of HF-HNO₃ acids. After five days of digestion, the

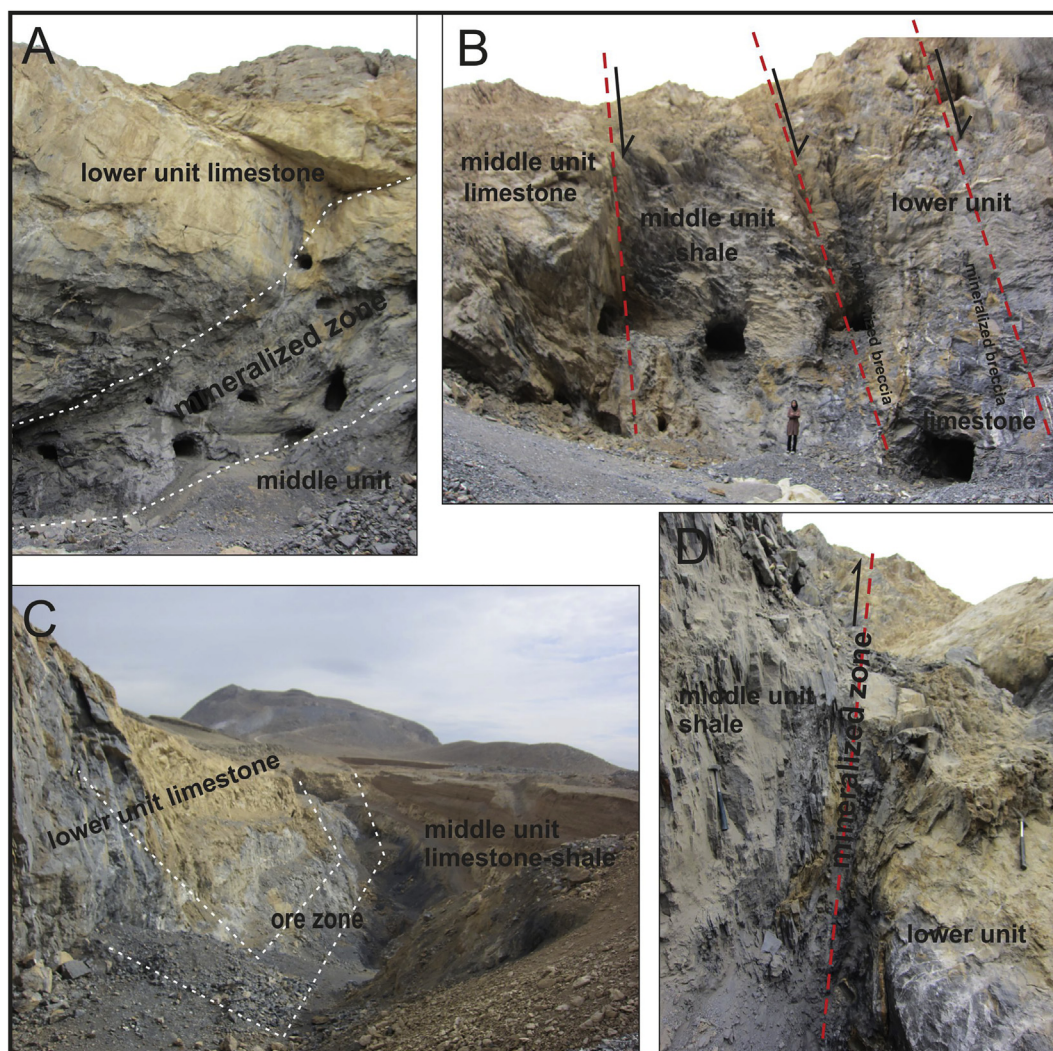


Fig. 6. Photographs of mineralization limited to the faults and fissures in shale-limestone contact zones, which is delineated by dashed lines and fault symbols and show displacement. a and b) Check-Ab orebody, c) Vejin-e-Bala orebody, and d) Old Anjireh orebody.

solution was evaporated to dryness and was then placed in 6 N HCl for two days. The solution was then evaporated again and placed in HBr. Pb elution and recuperation was achieved using standard anionic HBr-HCl chromatography. All reagents were purified by sub-boiling to minimize contamination. All isotopic ratios were obtained using a multicollector Finnigan Mat 262 mass spectrometer in static mode. All reported Pb isotopic ratios were corrected for mass fractionation by a factor of 0.129% per amu, obtained by measuring the deviation from repeated ($n = 11$) analyses of the NBS 981 standard. In-run precisions for all isotopic ratios are given at a 95% confidence level.

5. Results

5.1. Composition of Sphalerite and Galena

Selected samples of massive, breccia, vein, and disseminated sphalerite and galena from different orebodies showed no significant differences in their major- and trace-element composition. Iron, Cd, and Ag contents of sphalerite had maximum values of 4567, 2451, and 25 ppm, respectively. The silver, Sb, and Cu contents in the galena samples were low and reach up to 157, 375, and 472 ppm, respectively (Table 1).

5.2. Fluid inclusion studies

Microthermometric measurements were conducted on the red and yellow sphalerite, quartz (stage II), and late-stage calcite inclusions from the Chek-Ab, Old Anjireh, Vajin-e-Pain, and Tire-Vejin orebodies. Samples were selected based on each of the mineralization types, including veins and disseminated crystals. Table 5 summarizes the microthermometric data of the fluid inclusions. Irregularly distributed fluid inclusions, being isolated from adjacent and intercrystalline growth zone inclusions (Fig. 8), were the empirical criteria for discerning primary inclusions (Roedder, 1984). Two types of fluid inclusions were distinguished in the Tiran samples: two-phases (L + V) and one-phase (L) fluid inclusions. One-phase inclusions were mainly concentrated along healed fractures and were pseudosecondary or secondary in origin. All homogenization temperatures (T_h) and salinity measured from the inclusions were two-phases at room temperature. Fluid inclusions were mostly less than 10- μm -wide (Table 2). In these two-phases inclusions, liquid was dominant over vapor (liquid/vapor ratios ~ 0.85).

The salinity and T_h of primary fluid inclusions showed no significant differences between the vein and disseminated types. Initial ice melting temperatures (T_e) in sphalerite, quartz, and calcite inclusions vary between -53°C and -48°C . These low temperatures of first melting suggested the presence of some divalent cations, e.g., Mg and

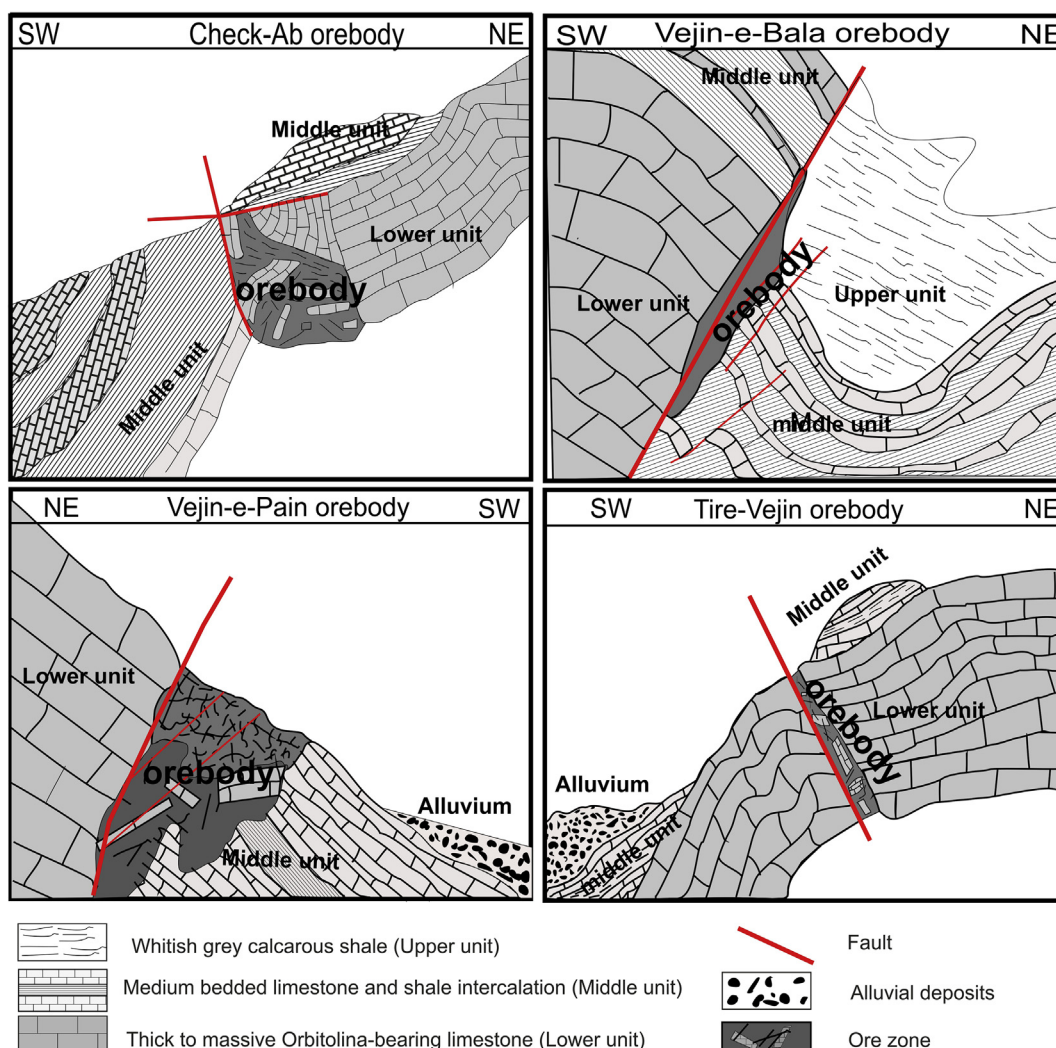


Fig. 7. Schematic cross sections (no scale) of the different Tiran ore deposits. a) Check Ab, b) Vejin-e-Bala, c) Vejin-e-Pain, and d) Tire-Vejin, which are modified after Lisenbee and Uzunlar (1988). The red lines demarcate bounding structures.

Ca. The measured eutectic temperatures were close to eutectic point for the NaCl-CaCl₂-H₂O system (Davis et al., 1990; Goldstein and Reynolds, 1994; Dubois and Marignac, 1997).

No carbonic-bearing inclusions or clathrates were observed in all of fluid inclusions. Final ice melting temperatures of selected inclusions

range between -5.4 and -18.4 °C indicating salinity vary from 8.6 to 21.2 wt% NaCl. The salinity of red and yellow sphalerite range from 15.9 to 20.6 wt% and 12.8 to 21.2 wt% NaCl_{equiv.} (average 19.2 and 18.7 wt% NaCl_{equiv.}), respectively. These values were higher than for salinity of quartz (8.5 to 19.4 wt% NaCl_{equiv.}, an average of 12.5 wt%

Table 1
Comparison of trace elements content (ppm) in red and yellow sphalerite (n = 8) and galena types (n = 6) of the Tiran Zn-Pb mining district.

Sample No	Orebody	Ore mineral	Ore texture	Trace elements frequency (ppm)								
				Fe	Cd	Ge	Ga	Cu	Ag	Pb	Sb	As
S-1	Chek-Ab	Red sph.	Vein	4567	1975	3	5	426	24.2	2292	304	4.6
S-2	Chek-Ab	Yellow sph.	Vein	3986	1754	4	4	473	25.7	2360	345	3.2
S-3	Chek-Ab	Red sph.	Disseminated	4174	2451	2	6	519	23.8	2451	322	3.9
S-4	Chek-Ab	Yellow sph.	Disseminated	3845	1784	3	5	442	24.1	2384	376	4.5
S-5	Chek-Ab	Galena	Vein	524	9.38	< 1	< 1	472	140	> 10	360	< 0.1
S-6	Chek-Ab	Galena	Disseminated	622	8.26	< 1	< 1	453	157	> 10	375	< 0.1
S-7	Vejin-e-Pain	Yellow sph.	Breccia	5213	2158	4	5	538	25.3	2357	328	4.5
S-8	Vejin-e-Pain	Yellow sph.	Disseminated	4536	2316	2	6	464	24.6	2156	364	5.2
S-9	Vejin-e-Pain	Galena	Breccia	548	7.56	< 1	< 1	492	195	> 10	328	0.2
S-10	Vejin-e-Pain	Galena	Disseminated	618	8.15	< 1	< 1	326	143	> 10	422	0.2
S-11	Tire-Vejin	Red sph.	Massive	3662	1843	3	6	295	20.6	2462	319	3.8
S-12	Tire-Vejin	Yellow sph.	Massive	3749	1952	3	4	456	24.5	2138	416	3.4
S13	Tire-Vejin	Galena	Massive	496	6.18	< 1	< 1	443	149	> 10	362	1.3
S-14	Tire-Vejin	Galena	Disseminated	534	9.61	< 1	< 1	381	173	> 10	381	< 0.1

Table 2

Microthermometric data from fluid inclusions in the Zn-Pb Tiran mining district.

Sample	Shape	Occurrence	Size	T _{fm} °C	Salinity (wt% NaCl equiv.)	Th (°C)
T1-Sph-r	Irregular	Cluster	5.8	-49.4	20.9	151.6
T1-Sph-r	Elongate	Random	8.7		20.7	155.5
T1-Sph-r	Irregular	Isolate	5.4		16.8	195
T1-Sph-r	Irregular	Isolate	6.9		20.4	136.8
T1-Sph-r	Elongate	Isolate	7.8	-51.5	16.8	183.1
T1-Sph-r	Oval	Cluster	8.1		19.7	153.9
T1-Sph-r	Spherical	Cluster	5.2		18.5	196.6
T2-Sph-Y	Irregular	Random	4.4	-53	17.8	152.4
T2-Sph-Y	Elongate	Isolate	5	-52.1	13.7	158.4
T2-Sph-Y	Irregular	Isolate	4.7		19.2	145.5
T2-Sph-Y	Elongate	Isolate	5.6		15.3	159.6
T3-Sph-r	Spherical	Isolate	6.7	-48.2	19.8	169.1
T3-Sph-r	Oval	Random	8.1		18.9	168.9
T3-Sph-r	Elongate	Random	3.9		19.8	154.6
T3-Sph-r	Elongate	Random	6.8		19.7	154.3
T3-Sph-Y	Elongate	Random	8.4	-47.6	21.2	141.4
T3-Sph-Y	Spherical	Random	5.4		20.7	139.2
T3-Sph-Y	Oval	Random	5.1		21.1	142.7
T3-Sph-Y	Elongate	Isolate	9.6		12.9	179
T4-Sph-Y	Elongate	Isolate	5	-52.8	17.4	150.9
T4-Sph-r	Irregular	Isolate	6.2		15.9	181.5
T4-Sph-r	Oval	Isolate	7.5		20.6	125.1
T4-Sph-r	Elongate	Isolate	4.8		19.6	137.2
T4-Sph-Y	Spherical	Random	4.2		18.7	154.5
T4-Sph-Y	Spherical	Random	3.3	-52.7	19.8	143.7
T4-Sph-Y	Spherical	Isolate	5.9		20.4	146.8
T4-Sph-Y	Spherical	Isolate	9		16.8	176.1
T4-Sph-r	Irregular	Cluster	8.4		19.7	153.9
T4-Sph-r	Oval	Cluster	6.6	-51.9	21	164.9
T4-Sph-r	Oval	Cluster	8.7		17.8	172.1
T5-Sph-r	Spherical	Isolate	4.9		19.9	147.4
T5-Sph-r	Spherical	Cluster	8.1		19.2	155.8
T5-Sph-r	Elongate	Random	5.5	-50.4	18.3	149.6
T5-Sph-r	Spherical	Random	7.1		18.5	167.2
T5-Sph-r	Spherical	Isolate	6.2		20.9	120.1
T6-Sph-Y	Elongate	Isolate	4.8		20.8	146.3
T6-Sph-Y	Irregular	Random	6.5		19.7	144.3
T6-Sph-Y	Irregular	Random	9.1		12.8	173.8
T6-Sph-Y	Spherical	Cluster	5.9	-49.8	20.7	119.2
T6-Sph-Y	Elongate	Isolate	8		15.4	152.7
T7-Sph-Y	Elongate	Isolate	6.3		20.1	129
T7-Sph-Y	Spherical	Cluster	5.1		17.4	110.9
T7-Sph-Y	Spherical	Random	3.9		16	181.5
T7-Sph-Y	Spherical	Random	8.5		19.2	125.1
T7-Sph-Y	Elongate	Random	14.4		20.7	168.2
T7-Sph-Y	Irregular	Random	6.8	-51.9	19.5	159.6
T7-Sph-Y	Irregular	Isolate	6.6		17.6	165.1
T8-Quartz	Spherical	Cluster	8.4		10.9	225.2
T8-Quartz	Elongate	Isolate	4.1		15.6	171.6
T8-Quartz	Irregular	Cluster	9.3		10.6	187.8
T8-Quartz	Irregular	Cluster	5.6	-47.9	9.1	198.4
T8-Quartz	Elongate	Isolate	7.2		10.7	185.2
T8-Quartz	Spherical	Isolate	3.8		10.4	178.3
T8-Quartz	Elongate	Random	7.8		14.1	193.2
T8-Quartz	Elongate	Random	9.2		19.9	143.2
T8-Quartz	Elongate	Isolate	15.4		10.2	187.8
T9-Quartz	Spherical	Random	4.5		10.3	189.3
T9-Quartz	Spherical	Isolate	7.1		8.9	191.5
T9-Quartz	Irregular	Random	4	-51.6	13.5	198.5
T9-Quartz	Irregular	Isolate	5.2		17.4	153.1
T9-Quartz	Spherical	Cluster	4.8		13.9	194.7
T6-Quartz	Irregular	Cluster	9		10.9	198.4
T6-Quartz	Elongate	Isolate	3.8	-50.3	12.7	184.9
T6-Quartz	Elongate	Isolate	10.1	-53.1	13.4	143.3
T6-Quartz	Irregular	Random	5.4		18.4	161.6
T6-Quartz	Elongate	Cluster	8.3		8.6	187.8
T6-Quartz	Irregular	Isolate	15.8	-52.7	10.1	195.4
T6-Quartz	Elongate	Isolate	10.7		12.8	205.9
T9-Calcite	Irregular	Random	6.8		10.9	208.1
T9-Calcite	Irregular	Cluster	11.2	-52.3	12.6	145.1
T9-Calcite	Elongate	Cluster	8.3		9.5	195.6
T9-Calcite	Irregular	Isolate	5.9		16.9	158.2

Table 2 (continued)

Sample	Shape	Occurrence	Size	T _{fm} °C	Salinity (wt% NaCl equiv.)	Th (°C)
T9-Calcite	Elongate	Isolate	5.6		10.3	154.6
T9-Calcite	Elongate	Isolate	6.3		15.4	121.2
T9-Calcite	Irregular	Random	5.3	-48.6	13.1	148.7
T5-Calcite	Irregular	Isolate	11.2		16.3	161.6
T5-Calcite	Elongate	Random	8.3		10.8	171.7
T5-Calcite	Irregular	Isolate	7		10.8	197.3
T5-Calcite	Elongate	Random	8.6		11.3	177.6
T5-Calcite	Elongate	Isolate	6.6		13.4	162.5
T5-Calcite	Irregular	Isolate	12.2		17.2	151.3
T5-Calcite	Elongate	Random	5.4		8.6	187.8
T5-Calcite	Irregular	Isolate	5.6		10.1	188.4
T5-Calcite	Elongate	Random	5.6	-48.7	12.1	145.3
T5-Calcite	Irregular	Cluster	7.8		20.2	155.4
T5-Calcite	Elongate	Cluster	14.2		8.9	192
T5-Calcite	Irregular	Cluster	4.7		10.7	174.8
T5-Calcite	Elongate	Isolate	8.6		19.9	165.3

NaCl_{equiv.}) and also higher than the salinity of calcite-hosted fluid inclusions that were 8.6 to 16.3 wt% with an average of 13.0 wt% NaCl_{equiv.}

The homogenization temperatures (Th) of the fluid inclusions vary between 111 and 208 °C, although majority of the Th values range between 140 and 190 °C. Average Th values in the red sphalerite, yellow sphalerite, quartz, and calcite were 158.8, 150.6, 184.5, and 168.1 °C, respectively (Fig. 9). The average homogenization temperature of fluid inclusions hosted by late-stage yellow sphalerite (150.6 °C) was slightly lower than for earlier red sphalerite (158.8 °C). The average homogenization temperature of the sphalerite-hosted inclusions (154.7 °C) was lower than that of homogenization temperatures of quartz (184.5 °C) and calcite-hosted inclusions (168.1 °C).

5.3. Sulfur isotope geochemistry

Fourteen mineral samples of vein- and disseminated-type of pyrite, sphalerite, galena, and barite from various generations of mineralization of the Tiran deposit were analyzed for sulfur isotopes (Table 3). The $\delta^{34}\text{S}$ determined from separated grains from the vein-type samples range from -8.9 to +1.3‰ and the disseminated-type samples vary from -8.2 to +4.2‰. Although there was a wider range of $\delta^{34}\text{S}$ values for disseminated-type minerals, $\delta^{34}\text{S}$ values of both types are not significantly different. The $\delta^{34}\text{S}$ for the galena samples vary between -8.9 and -1.1‰, averaging -5.6‰. The $\delta^{34}\text{S}$ values of the sphalerite samples range from -7.2 to -1.0‰, averaging -2.9‰, and the pyrite samples range from -6.2 to +4.15‰ (averaging 1.4‰). Barite samples displayed a narrow range of $\delta^{34}\text{S}$ from +22.6 to +23.9‰ (Fig. 10). Fractionation factors proposed by Ohmoto and Rye (1979) were used to calculate the mineralization temperature (see also Seal, 2006). The calculated temperatures for two coexisting sphalerite-galena mineral pairs (contiguous crystals) were 187° and 177 °C. These calculated temperatures fall in the range of homogenization temperatures for fluid inclusions.

5.4. Lead isotopes

Lead isotope measurements for the galena and sphalerite samples are shown in Table 4. The $^{206}\text{Pb}/^{204}\text{Pb}$, $^{207}\text{Pb}/^{204}\text{Pb}$, and $^{208}\text{Pb}/^{204}\text{Pb}$ ratios range from 18.1 to 18.4, 15.6 to 15.7, and 38.2 to 38.6, respectively. When plotted on the Pb-Pb diagrams of Zartman and Doe (1981), the Pb isotope data were co-linear showing a positive correlation on the thorogenic isotope plot, but they were more scattered on the uranogenic diagram (Fig. 11). The trend showed a natural scatter as the individual errors represented less than twice the 2 σ analytical uncertainty. The μ values of Pb isotopes ($^{238}\text{U}/^{204}\text{Pb}$) range from 9.85 to

Table 3

Sulfur isotope data (V-CDT, ‰) from separates of sphalerite, galena, pyrite, and barite of the Tiran Zn-Pb mining district.

Sample No	Single crystal	Orebody	δS^{34} (‰)	Th (°C)
12	Vein type galena, fine grain (~0.2 mm)	Chek Ab	-8.92	-
21	Vein type sphalerite, red, relatively fine grain (~0.4 mm)	Chek Ab	-7.19	-
8	Vein type pyrite, relatively fine grain (< 0.4 mm), ore stage pyrite	Chek Ab	-6.22	-
13	Vein type galena (II), medium grain (~0.6 mm)	Vejin-e-Bala	-4.47	186.5
22	Vein type sphalerite, yellow, medium grain (~1 mm)	Vejin-e-Bala	-1.02	-
9	Vein type pyrite, late stage, coarse grain	Vejin-e-Bala	1.28 +	-
14	Disseminated galena, main stage (galena I), fine grain (~1 mm)	Tire-Vejin	-1.12	51.6
23	Disseminated sphalerite, red, relatively fine grain (> 0.4 mm)	Tire-Vejin	-8.04	-
10	Disseminated pyrite, late stage, coarse grain (~2 mm)	Tire-Vejin	4.15 +	-
15	Disseminated galena, relatively fine grain (< 0.5 mm)	Vejin-e-Pain	-8.24	176.5
24	Disseminated sphalerite, red, medium grain (1.0 mm)	Vejin-e-Pain	-4.63	-
11	Disseminated pyrite, main stage, medium grain (~0.5 mm)	Vejin-e-Pain	-4.65	-
29	Barite, fracture filling	Vejin-e-Bala	22.61 +	-
30	Barite, vein filling	Vejin-e-Bala	23.88 +	-

10.15 and continued to show more radiogenic values on the $^{206}\text{Pb}/^{204}\text{Pb}$ diagram (Table 4, Fig. 11).

6. Discussion

6.1. Structural and stratigraphic controls on fluid flow

During the mineralization of MVT deposits, the main features governing fluid flow and the location of ores are porosity-permeability and the fluid conduits, important for controlling the rate and volume of fluid flow. For example, normal faults are one of the most important ore controls, producing fractures and related dilatancy zones (Kibitlewski, 1991; Leach and Sangster, 1993; Clendenin et al., 1994; Hitzman, 1999; Hudson, 2000; Wight et al., 2003; Leach et al., 2005). Shale depositional edges and shale-carbonate transitions also tend to act as aquitards, inhibiting fluid flow, and producing a trap that results in changing the physicochemical conditions of the fluid(s) (Anderson, 1975; Deloule and Turcotte, 1989; Person and Garven, 1994; Leach et al., 2005; BouAbdellah et al., 2012).

In the Tiran district, ore deposits are limited to a series of relay

zones along the migration path to channel fluid flow. Mineralization occurred in the crushed zone of lower and middle unit carbonates constrained by impermeable clay-rich strata. Strike-slip faulting and associated cataclastic zones provide zones of greater dilatancy and permeability, thereby reducing fluid pressure (Ghazban et al., 1994; Rowan and Goldhaber, 1995; Roberts et al., 1996; Keyser and Hiatt, 2003). Pb-Zn deposits of the Tiran district formed when metal-bearing fluids moved through the faulted carbonates favoring the precipitation of ore minerals.

Stratigraphic contacts favored certain horizons including crushed carbonates restricted by impermeable clay-rich strata. These impermeable strata limited hydrothermal fluid flow out of the faulted zone. In addition to shale strata's impermeable features, these strata are also organic-rich and provide an ideal geochemical environment to inorganically reduce sulfur. Fluid migrated along the strike-slip fault and probably encountered different geochemical conditions that promoted mineralization. Variation in the thickness of the different orebodies suggests that fluid flow was not uniform and that mineralization was more evolved in most brecciated and displacement zones.

Table 4

Lead isotope compositions of galena and sphalerite samples of the Tiran mining district and some surrounding SSZ deposits (Emarat deposit: Ehyah et al. (2010); Ahangaran, Kohkolangeh, Tapeh Sorkh, Kolah Darvazeh, Doshkharat, Dareh Noghreh, Babsheikh, Chah Talkh, and Saleh Peighambar: Mirnejad et al. (2011) are given for comparison.

Sample No.	$^{208}\text{Pb}/^{204}\text{Pb}$	$^{207}\text{Pb}/^{204}\text{Pb}$	$^{206}\text{Pb}/^{204}\text{Pb}$	μ	Description
<i>This study</i>					
S1	38.238	15.690	18.060	10.15	vein type galena, Vejin-e-Bala
S2	38.237	15.687	18.066	10.15	vein type sphalerite, Vejin-e-Bala
S3	38.577	15.646	18.395	9.85	disseminated galena, Tire-Vejin
S4	38.507	15.661	18.316	9.85	disseminated sphalerite, Tire-Vejin
S5	38.262	15.698	18.068	10.15	disseminated galena, Vejin-e-Pain
S6	38.560	15.641	18.392	9.87	vein type galena, Check-Ab
<i>Ehyah et al. (2010)</i>					
GEF1	39.14	15.64	18.62	9.8	Galena, Emarat deposit
GEF2	39.22	15.77	18.57	10.3	Galena, Emarat deposit
GEF3	39.21	15.68	18.58	9.98	Galena, Emarat deposit
GEF4	39.98	15.65	18.56	9.86	Galena, Emarat deposit
GEF5	38.69	15.58	18.45	9.58	Galena, Emarat deposit
GEF6	38.64	15.57	18.55	9.52	Galena, Emarat deposit
<i>Mirnejad et al. (2015)</i>					
Ahangaran	18.407	15.641	38.57	9.85	Galena, Ahangaran deposit
Kohkolangeh	18.389	15.628	38.47	9.81	Galena, Kohkolangeh deposit
Tapeh Sorkh	18.45	15.651	38.63	9.89	Galena, Tapeh Sorkh deposit
Kolah Darvazeh	18.419	15.634	38.56	9.83	Galena, Kolah darvazeh deposit
Doshkharat	18.44	15.659	38.64	9.93	Galena, Doshkharat deposit
Dareh Noghreh	18.398	15.64	38.49	9.86	Galena, Dareh noghreh deposit
Babsheikh	18.424	15.646	38.54	9.88	Galena, Babsheikh deposit
Chah Talkh	18.454	15.635	38.60	9.82	Galena, Chah talkh deposit
Saleh Peighambar	18.471	15.652	38.65	9.89	Galena, Saleh peighambar deposit

Table 5
Summary of microthermometric and salinity data of mineralization in the Tiran mining district.

Host mineral	Inclusion type	Te (°C)	Th (°C)	Salinity (wt% NaCl eq.)	n
Vein type sphalerite (Red)	L + V	−49.4/51.5	125.1–196.6	15.9–20.9	14
Disseminated sphalerite (Red)	L + V	−48.2/−51.9	120.1–172.1	16.8–21.0	8
Vein type sphalerite (Yellow)	L + V	−47.6/53	139.2–179.0	12.9–21.2	15
Disseminated sphalerite (Yellow)	L + V	−49.8/−51.9	119.2–181.5	12.8–20.7	10
Vein type Quartz	L + V	−52.3/−53.1	143.2–225.2	8.9–19.9	10
Disseminated Quartz	L + V	−47.9/−52.1	143.3–205.9	8.6–18.4	11
late stage Calcite	L + V	−48.6/−52.3	121.2–208.1	8.6–19.9	20

Notes: Te: first ice melting; Th: homogenization to liquid; n: number of measurements.

6.2. Trace-element content in sphalerite and galena

Preliminary trace element data for sphalerite and galena samples ($n = 14$) from the Tiran deposits showed no significant differences between the trace element content of vein- and disseminated-type minerals (Table 1). Trace element contents of sphalerite and galena occur mainly as solid solution and micro-inclusions of minerals (Cook et al., 2009; Lin et al., 2011; Lockington et al., 2014; Jazi et al., 2017). The advantage of determining of trace elements in sulfide minerals is that they show fractionation of trace elements as a function of temperature and metal sources (Scott and Barnes, 1971; Kramer et al., 1987; Di Benedetto et al., 2005; Cook et al., 2009). In the Tiran mining district, the similarity between trace element contents suggests the vein- and disseminated-type sulfides derived their metal contents from a single metal-bearing parent fluid and/or physical-chemical conditions of sulfide deposition are similar. The low Ag, Cu, and Sb values in galena are typical for a low-temperature ore formation (sediment-hosted Pb-Zn deposits), e.g., MVT, Irish, and SEDEX deposits (Dill et al., 2011). MVT deposits typically have lower Ag values than those of SEDEX deposits (Gustafson and Williams, 1981). Sphalerite samples from different types of deposits are refractory minerals and their trace elements are as a tracer for ore genesis (Lin et al., 2011). Sphalerite samples of Tiran district contained elevated Cd (2290–2451 ppm) and low Fe ($< 0.5\%$),

Ge (< 4 ppm), and Ga (< 6 ppm) values; results similar to those found in low-temperature Pb-Zn deposits (Gustafson and Williams, 1981; Leach and Sangster, 1993; Peevler et al., 2003; Dill et al., 2008). The chemical composition of analyzed sulfide minerals from Tiran closely resemble carbonate-hosted MVT deposits, e.g., Upper Silesia, Poland, and Wiesloch, Germany (Peevler et al., 2003; Dill et al., 2008; Dill, 2010). This would suggest that ore mineralization took place from low-temperature fluids under depositional conditions typical of MVT mineralization.

6.3. Fluid source and physicochemical conditions of metal solubility

Fluid inclusion microthermometry shows that two fluids, having a composition similar to that of basinal brines, were incorporated in the Tiran district mineralization. Ore deposition occurs when two NaCl–CaCl₂-bearing fluids (eutectic point -53 to -48 °C) having a high (19 wt% NaCl_{equiv.} and Th: 154.7 °C) and a medium salinity (12.5 wt% NaCl_{equiv.} and Th: 70–250 °C) are mixed together (Fig. 12). Basinal brines in sedimentary basins are highly mobile, thus leading to extensive mixing of different basinal brines (Hitchon and Friedman, 1969; Kharaka and Carothers, 1986; Worden et al., 1999; Ziegler and Coleman, 2001; Kharaka and Hanor, 2007). The mixing of two basinal brines with different salinity, redox condition, metal and S contents

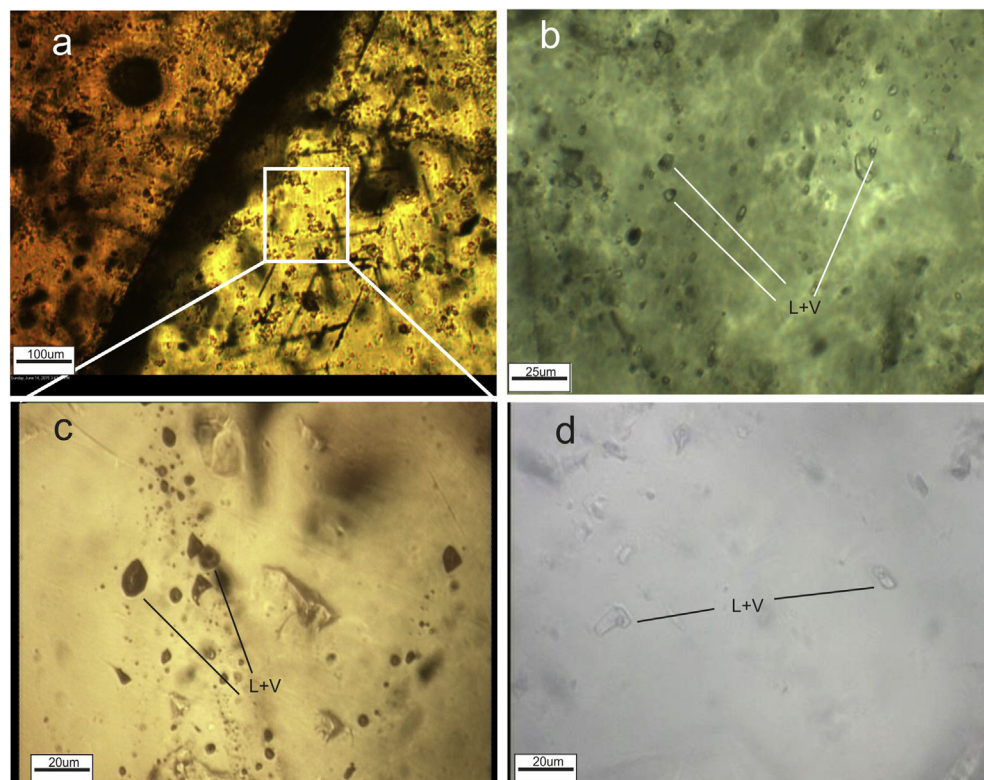


Fig. 8. Photomicrographs in transmitted PP light of fluid inclusion types in sphalerite, quartz, and calcite from the different deposits in the Tiran mining district. a) Primary fluid inclusions in red (left hand) and yellow (right hand) sphalerite (deposit). b) Two-phase liquid and gas fluid inclusion trapped in calcite (Chek Ab deposit). c) Enlargement of (a). d) Two-phase liquid and gas fluid inclusion trapped in quartz (Old Anjireh deposit).

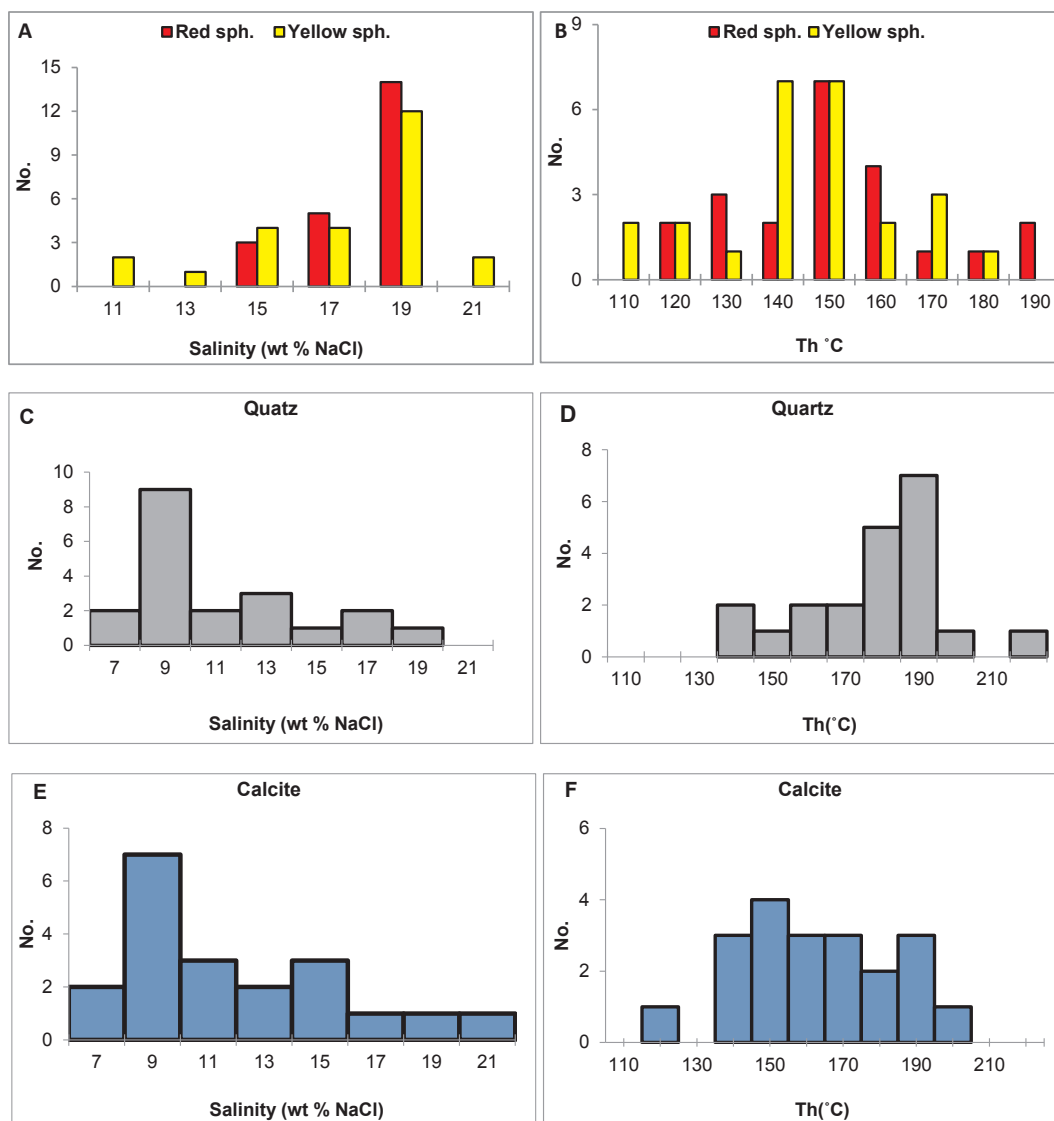


Fig. 9. Homogenization temperature (A: in sphalerite, B in quartz and C in calcite fluid inclusions) and salinity (D: in sphalerite, E in quartz, and F in calcite fluid inclusions) histograms of fluid inclusion at the Tiran mining district.

play an important role in the precipitation of ore and gangue minerals in MVT deposits (Sverjensky, 1984; Saunders and Swann, 1990; Leach and Sangster, 1993; Corbella et al., 2004; Adams et al., 2000; Kharaka and Hanor, 2007). Fig. 13 shows a decreasing trend of salinity and temperature. The first fluid, detected in sphalerite-hosted inclusions and marked by higher salinity (18.7 wt% NaCl_{equiv.}), and lower temperature (Th: 154.7 °C), fall in the middle of the salinity and temperature range of MVT fluids (salinity: 10–30 wt% NaCl_{equiv.} and Th: 70–250 °C). The second fluid, found in quartz-hosted inclusions, fall in the lower range for salinity and temperature of MVT fluids (Leach et al., 2005; Shelton et al., 2009; Bodnar and Lecumberri-Sanchez, 2014). Mixing of two basinal brines may have been favored by deposition of calcite having a moderate salinity and homogenization temperature (average salinity: 13 wt% NaCl_{equiv.} and Th: 168 °C).

In sedimentary basins, salinity increases with depth, however, the origin of brines having a high salinity remains controversial (Hanor, 1994; Bazin et al., 1997; Kharaka and Hanor, 2007; BouAbdellah et al., 2012). Most published studies favor the evaporation of seawater, dissolution of halite, or dispersive mixing of fluids in subsurface environments as being the source of basinal brine salinity (Rittenhouse, 1967; Hanor, 1994; Kesler et al., 1996; Bazin et al., 1997; Kharaka and Hanor, 2007). The electrolyte composition of the fluid inclusions found

in the sphalerite of the MVT deposits suggests that the ultimate source of mineralized fluids was seawater evaporation. However, minor contributions from halite dissolution cannot be excluded (Chi and Savard, 1997; Leach et al., 2005).

Hanor (1996) proposed that in ore-forming brines, transportation of Pb and Zn was mostly controlled by chloride complexes. A chloride threshold of 100 g·L⁻¹ (salinity ~17 wt% NaCl) was calculated for metal transportation in the basinal brines (at temperatures < 150 °C) when the reduced sulfur concentrations were lower than 0.02 mg·L⁻¹ (Kharaka et al., 1987; Sicree and Barnes, 1996; Giordano, 2000; Kharaka and Hanor, 2007). Therefore, it is reasonable to conclude that only the first fluid of the sphalerite-hosted inclusions contributed a high enough concentration of chloride (110 g·L⁻¹) to act as solvent for Pb and Zn. In the Tiran district, ore mineralization occurred due to fluid mixing/circulation in the crushed zone. Therefore, fluid mixing between lower and higher salinity fluids could change the environmental conditions of metal-bearing fluids by decreasing ligand activity and, as a result, the solubility of metals (Hanor, 2001). As such, we propose that dilution may have had an important role in metal deposition in the Tiran district. Precipitation of both quartz and sphalerite results from environmental changes triggered by temperature, salinity and reduced sulfur content (Viets and Leach, 1990; Plumlee et al., 1994). Two

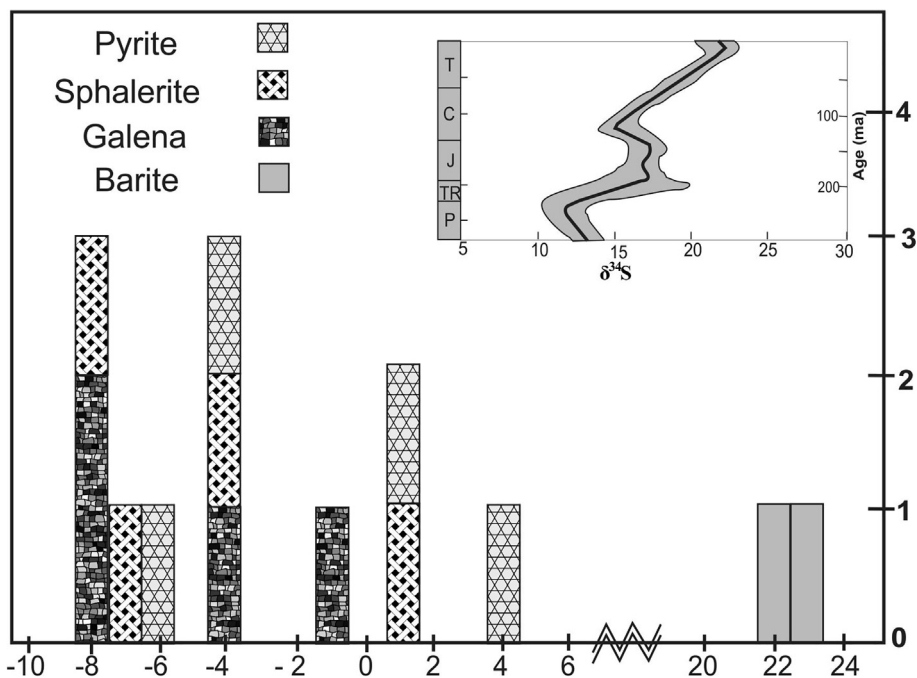


Fig. 10. $\delta^{34}\text{S}_{\text{V-CDT}}$ values (‰) of sulfur-bearing minerals (barite, galena, sphalerite, and pyrite) of the Tiran mining district, in comparison to $\delta^{34}\text{S}_{\text{V-CDT}}$ values of marine sulfates from the Permian to Tertiary (see Claypool et al., 1980).

formational fluids experienced different degrees of mixing during mineralization, resulting in the rhythmic deposition of ore and gangue minerals (quartz, sphalerite, and calcite) (Fig. 7).

6.4. Source of sulfur and mechanisms of sulfide deposition

Leach et al. (2005) proposed that one or more sources of crustal sulfur are possibly incorporated into MVT ore systems (Table 6). The main sources of sulfur are sulfate-bearing evaporates, dissolved marine

sulfates, sulfate derived by oxidation of sulfides, H_2S reservoir gas, and sulfur-bearing organic materials (Ohmoto and Rye, 1979; Sangster, 1990). The sulfate sources are subsequently reduced to hydrogen sulfur. Two explanations have been proposed to explain sulfur reduction in MVT deposits (Peevler et al., 2003): bacterially-mediated sulfate reduction (BSR) and thermochemical sulfate reduction (TSR). BSR is normally depleted in $\delta^{34}\text{S}$ relative to a sulfate source (from 15 to 60‰) and varies across a vast negative range (Hitzman and Beaty, 1996). TSR at higher temperatures, in the presence of organic matter, produces $\delta^{34}\text{S}$

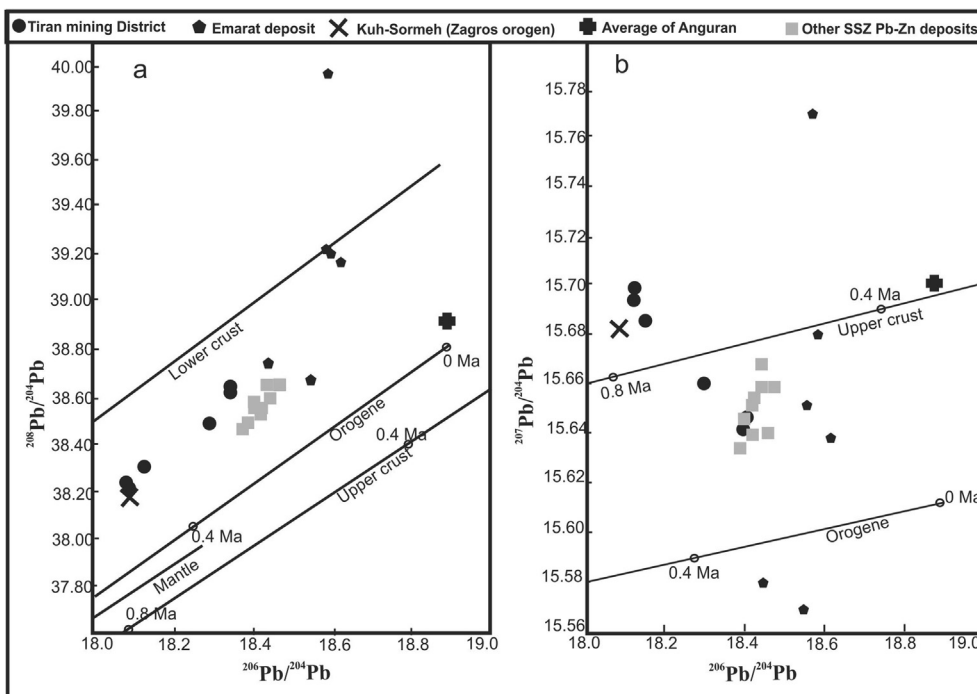


Fig. 11. Plot of Pb isotope ratios of the Tiran mining district on the plumbotectonic diagrams (Zartman and Doe, 1981). Pb isotope data for Emarat deposit are after Ehya et al. (2010); Kuh-Sormeh and other Pb-Zn deposits of SSZ after Mirnejad et al. (2011) are given for comparison.

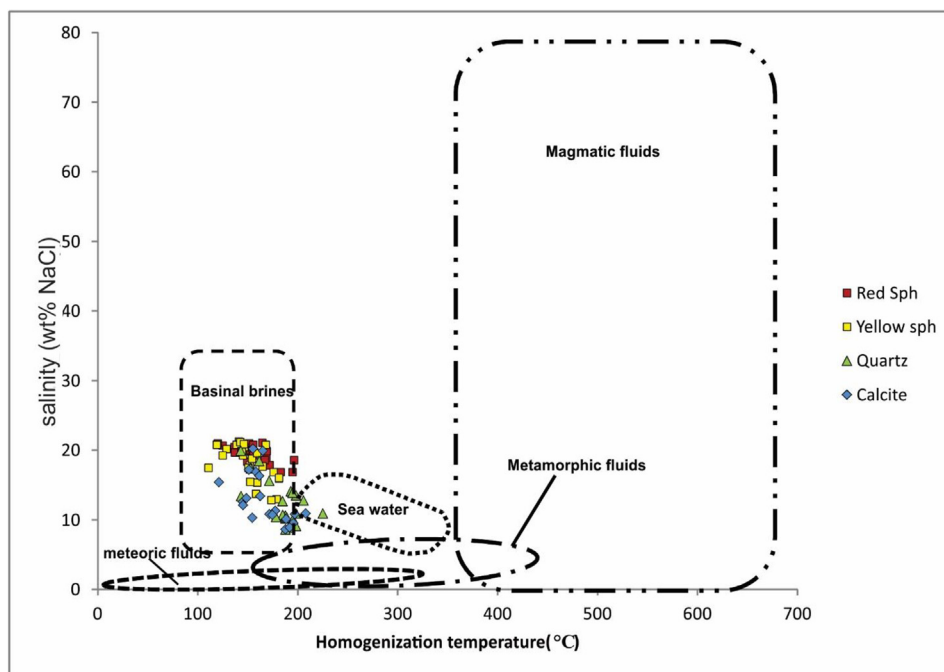


Fig. 12. Homogenization temperature vs. salinity diagram show that fluid inclusion of ore and gangue minerals of the Tiran mining deposits plotted in the basinal brines area; however calcite and quartz fluid inclusions have shown a trend to sea water (see Kesler, 2005).

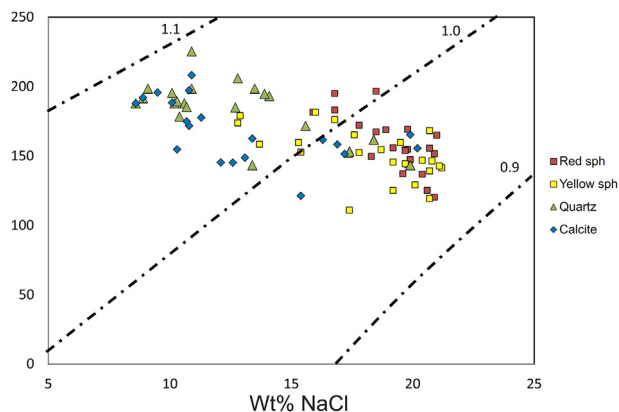


Fig. 13. Homogenization temperature (Th) vs. salinity diagram of the Tiran mining district fluid inclusions. The dashed lines show densities (g/cm³) of fluid inclusions (modified after Wilkinson, 2001).

values similar to the parent sulfate extending up to -15‰ (Anderson, 1991; Ohmoto and Goldhaber, 1997; Machel, 2001; Seal, 2006).

The δ³⁴S values for the sphalerite and galena samples of the Tiran

district ores are negative (-8.9 to -1.0‰), whereas pyrite samples show a range of negative to positive values (-6.2 to +4.2‰). The broad range of δ³⁴S values for the Tiran sulfide minerals (-8.9 to +4.2‰) suggest multiple sources of sulfur involved during mineralization (two sulfur end-members). In the Tiran system, negative values would appear to be due to BSR and the low positive values due to a mixing of TSR and BSR sources. A mixing trend in the Tiran samples is shown by isotopic data (Fig. 10). This data is consistent with fluid mixing between a metalliferous, sulfate-bearing fluid and a H₂S-rich fluid (Barrett and Anderson, 1982; Anderson and Garven, 1987; Anderson, 1991; Appold and Garven, 2000; Peevler et al., 2003; Appold and Wenz, 2011). Furthermore, it is possible that light isotopic sulfur was released from the thermal degradation of pyrite in shale (e.g. Jurassic shales or Cretaceous shale-bearing strata). The calcareous shale and mud of the Cretaceous sequences are enriched in diagenetic pyrite. The leaching of this pyrite near the mineralization site in faulted shale-limestone contacts offers a significant source of reduced sulfur (Phillips and Evans, 2004; Decrée et al., 2008), however the δ³⁴S values of this diagenetic pyrite are not available to confirm this hypothesis.

The complex evolution of sulfide texture matches the sulfur isotopes. If a fluid is supersaturated with respect to reduced sulfur, it typically results in fine-grained sulfide deposition (inferred to be rapid),

Table 6
Comparison of Zn-Pb mineralization in the Tiran mining district with other Pb-Zn deposits worldwide.

Deposit	Host rock	Deposition mechanism	Th °C	Salinity wt% NaCl equiv.	Mineralization type	Reference
Irish deposits	Carbonates	Fluid mixing	90–270	4–28	Irish	Wilkinson (2010)
Viburnum Trend	Carbonates	Fluid mixing	85–150	21–27	MVT	Rowan and Leach (1989)
N. Arkansas	Carbonates	Fluid mixing/water rock interaction	100–140	16–25	MVT	Stoffell et al. (2008)
Appalachian belt	Carbonates	Fluid mixing	60–190	15–32	MVT	Williams-Jones et al. (1992)
Emarat (Iran)	Carbonates	Fluid mixing	90–250	1.7–15	MVT	Ehya et al. (2010)
Ravanj (Iran)	Carbonates	Fluid mixing	120–220	1–22	MVT	Nejadhadad et al. (2015)
Irankuh (Iran)	Carbonates	Fluid mixing/water rock interaction	80–166	–	MVT	Ghazban et al. (1994); Hosseini-Dinani and Aftabi (2016)
Angouran	Carbonate	water rock interaction	170–80	23–25	MVT	Gilg et al. (2006)
Tiran district	Carbonates	Fluid mixing	111–225	8.6–21.2	MVT	This study

whereas undersaturated reduced sulfur should result in a low growth rate and produce coarse-grained textures (Anderson, 2008; Anderson and Thom, 2008). Therefore, BSR-generated H₂S in the fluid (−8.9‰) would have caused the deposition of fine-grained sulfide minerals, whereas low rate of TSR (+4.2‰) in the fluid produced low growth rates during sulfide deposition and thus medium- to coarse-grained pyrite (Table 3).

Claypool et al. (1980) detailed how δ³⁴S values of seawater changed through geological times (+10.5 to +31‰). The high positive δ³⁴S values of the Tiran barite samples (+22.6 to +23.9‰) suggest that early Tertiary marine sea water or Tertiary evaporitic sulfates (e.g. Lower Red Formation) were the sulfur source for the Tiran barite. Geological and textural evidence suggest a post-tectonic ore deposition for the Tiran deposits. In addition, sulfur isotopic data indicate that Tertiary marine sulfate was likely a significant source of sulfur. Thus, mineralization would be expected to be post-tectonic, probably late Cretaceous to early Tertiary, contemporaneous with orogenesis. This explanation suggests a post-tectonic mineralization, analogous to that described in the Appalachian Ba-Pb-Zn thrust belt (Williams-Jones et al., 1992).

Sulfur isotope fractionation of two galena-sphalerite pairs were 176 and 186 °C, near the mode of temperatures obtained by fluid inclusion microthermometry. However, the calculated temperature (~180 °C) is higher than that typical for bacterial activity. However, it is possible that BSR took place at a different place or time (Cooke et al., 2000; Giordano, 2002; Yardley, 2005; Leach et al., 2006; Wilkinson, 2010). If the temperature (~160 °C) is representative of mineralization, the δ³⁴S values of hydrogen sulfide equilibrated with sulfide minerals in ore-forming fluid vary from −5.6 to +7.8‰ (cf. Li and Liu, 2006).

6.5. Source of Pb

Tiran Pb isotope samples are characterized by limited variation in their compositions. On the thorogenic diagram, Pb compositions showed a positive linear correlation and were distributed between the lower and upper crust curves reflecting a mixing between multiple end-members (Fig. 11a). On the other hand, the uranium isotope diagram showed more complexity (Fig. 11b). The samples plotted between the orogen and upper crust curves, as well as above the upper crust curve, thus indicative of a heterogeneous source for Pb. These variations may reflect different crustal sources that contributed Pb to the mineralization site. However, like other Pb-Zn deposits of the SSZ and the Zagros Orogeny (Fig. 11), the ultimate source of Pb is crustal (Ehya et al., 2010; Mirnejad et al., 2011). Crustal sources of Pb were also reflected by higher U/Pb ratios, high ²⁰⁶Pb/²⁰⁴Pb ratios at the time of mineralization, determined from calculated μ values (Zartman and Doe, 1981). High μ values indicate a large contribution of radiogenic materials. The Pb isotope data may reflect surrounding or underlying lithology of the deposits (Goldhaber et al., 1994; Bouabdellah et al., 2012; Mirnejad et al., 2013). The Sanandaj-Sirjan Zone (SSZ) is predominantly comprised of deformed sedimentary rocks of the Zagros Orogeny and Mesozoic magmatic rocks, which may be the source of Zn, Pb, and Ag. Therefore, our Pb isotope data suggests an orogenic reservoir coupled with a large contribution from crustal basement rocks as metal sources for the Tiran deposits; a pattern similar to most MVT deposits (Leach et al., 2005).

7. Conclusions

This paper presents geological, textural, fluid inclusion, and S and Pb isotope data from the Tiran Zn-Pb district ore deposits. As most of the carbonate-hosted Pb-Zn deposits are found in the Sanandaj-Sirjan Metallogenic belt, Lower Cretaceous carbonates of the Tiran district are faulted during Upper Cretaceous and fluid flow was locally restricted by impermeable shaly strata. These structural and stratigraphical factors control reducing conditions for Tiran Pb-Zn mineralization. Fluid

inclusion studies of ore and gangue minerals revealed at least two geochemically distinct fluids that were basin-derived and warm. Fluid inclusions in sphalerite had a higher salinity than those of quartz-hosted inclusions although the average homogenization temperature of sphalerite-hosted inclusions was lower than quartz. This salinity-temperature pattern supports for the idea of fluid mixing. The sulfur isotope composition of sulfide minerals showed a wide range of values (−8.9 to +4.15‰). These values reflect a dominantly bacteriogenic origin with some contributions from thermochemical sulfate reduction. Barite sulfur isotope compositions, in contrast to sulfides, showed a narrow range (+22.6 to +23.9‰) reflecting a sulfate-rich brine derived from the Tertiary seawater or related formational brines in the overlying strata. The Pb isotopic data of the Tiran mining district supports multiple end-member sources, i.e. a heterogeneous Pb source. This study suggests crustal basement rocks, predominantly deformed sedimentary rocks of the Zagros Orogeny, are the source of Pb.

The geological setting and mineral paragenesis of the Tiran Zn-Pb mining district are comparable with most carbonate-hosted Mississippi-Valley-type deposits (Table 6). This model explains epigenetic mineralization events following host rock deformation during late Cretaceous or early Tertiary orogenesis. The mixing of two fluids along the faulted zone, locally restricted by impermeable shaly strata, led to increasing reduced sulfur, cooling, dilution, decreasing ligand activity, and ore deposition.

Acknowledgments

Authors acknowledge the financial support from the Research Committee of Shiraz University, Iran. The CEO of Tiran mine is thanked for providing unlimited access to the Tiran deposits. Fluid inclusion microthermometry was carried out in the laboratory of the Iran Mineral Processing Research Center (IMPRC). Contributions from M Aghajani, laboratory head of the fluid inclusion lab, are kindly acknowledged. DL was supported by a NSERC Discovery grant. Special thanks to Sherri Strong of Memorial University for her assistance with Pb isotope analyses. Special thanks is extended to Prof. Franco Pirajno Editor-in-Chief and Dr. Hooshang Asadi as Associate editor of the Journal of Ore Geology Reviews and one anonymous reviewer for their valuable and constructive comments to improving this manuscript.

Appendix A. Supplementary data

Supplementary data associated with this article can be found, in the online version, at <https://doi.org/10.1016/j.oregeorev.2018.08.005>.

References

- Adams, J.J., Rostron, B.J., Mendoza, C.A., 2000. Evidence for two-fluid mixing at Pine Point, NWT. *J. Geochem. Explor.* 69–70, 103–108.
- Agard, P., Omrani, J., Jolivet, L., Mouthereau, F., 2005. Convergence history across Zagros (Iran): constraints from collisional and earlier deformation. *Int. J. Earth Sci.* 94, 401–419.
- Alavi, M., 1994. Tectonics of Zagros Orogenic belt of Iran, new data and interpretation. *Tectonophysics* 229, 211–238.
- Alavi, M., 2004. Regional stratigraphy of the Zagros fold-thrust belt of Iran and its proforeland evolution. *Am. J. Sci.* 304, 1–20.
- Anderson, G.M., 1975. Precipitation of Mississippi valley-type ores. *Econ. Geol.* 70 987–942.
- Anderson, G.M., Garven, G., 1987. Sulfate-sulfide-carbonate associations in Mississippi Valley-type lead-zinc deposits. *Econ. Geol.* 82, 482–488.
- Anderson, G.M., 1991. Organic maturation and ore precipitation in Southeast Missouri. *Econ. Geol.* 86, 909–926.
- Anderson, G.M., 2008. The mixing hypothesis and the origin of Mississippi Valley-type ore deposits. *Econ. Geol.* 103, 1683–1690.
- Anderson, G.M., Thom, J., 2008. The role of thermochemical sulfate reduction in the origin of Mississippi Valley-type deposits. II. Carbonate-sulfide relationships. *Geofluids* 8, 27–34.
- Appold, M.S., Garven, C., 2000. Reactive flow models of ore formation in the Southeast Missouri district. *Econ. Geol.* 95, 1605–1626.
- Appold, M.S., Wenz, Z.J., 2011. Composition of Ore Fluid Inclusions from the Viburnum Trend, Southeast Missouri District, United States: implications for Transport and

- Precipitation Mechanisms. *Econ. Geol.* 106, 55–78.
- Barrett, T.J., Anderson, G.M., 1982. The solubility of sphalerite and galena in NaCl brines. *Econ. Geol.* 77, 1928–1983.
- Bazin, B., Brosse, E., Sommer, F., 1997. Chemistry of oil-field brines in relation to diagenesis of reservoirs: 1. Use of mineral stability fields to reconstruct in situ water composition. Example of the Mahakam basin. *Petrol. Geol.* 14, 481–495.
- Berberian, F., Berberian, M., 1981. Tectono-plutonic episodes in Iran. *Am. Geophys. Union Geodynamic Series* 3, 5–32.
- Berberian, M., King, G.C.P., 1981. Towards a paleogeography and tectonic evolution of Iran. *Can. J. Earth Sci.* 18, 210–265.
- Bodnar, R.J., 1993. Revised equation and table for determining the freezing point depression of H₂O–NaCl solutions. *Geochim. Cosmochim. Acta* 57, 683–684.
- Bodnar, R.J., Lecumberri-Sanchez, P., Moncada, D., Steele-MacInnis, M., 2014. Fluid inclusions in hydrothermal ore deposits. In: Holland, H.D., Turekian, K.K. (Eds.), *Treatise on Geochemistry*, second ed. Elsevier, Oxford, pp. 119–142.
- Bouabdellah, M., Sangster, D.F., Leach, D.L., Brown, A.C., Johnson, C.A., Emsbo, P., 2012. Genesis of the Touissit-Bou Bekker Mississippi valley-type district (Morocco-Algeria) and its relationship to the Africa-Europe collision. *Econ. Geol.* 107, 117–146.
- Chi, G., Savard, M., 1997. Sources of basinal and Mississippi Valley-type mineralizing brines; mixing of evaporated seawater and halite-dissolution brine. *Chem. Geol.* 143, 121–125.
- Claypool, G.E., Holser, I.R., Sakai, H., Zak, I., 1980. The age curves of sulfur and oxygen isotopes in marine sulfate and their mutual interpretation. *Chem. Geol.* 28, 199–259.
- Clendenin, C.W., Niewendrop, C.A., Duane, M.J., Lowell, G.R., 1994. The paleohydrology of Southeast Missouri Mississippi valley-type deposits, interplay of faults, fluids, and adjoining lithologies. *Econ. Geol.* 89, 322–332.
- Corbella, M., Ayora, C., Cardellach, E., 2004. Hydrothermal mixing, carbonate dissolution and sulfide precipitation in Mississippi Valley-Type deposits. *Miner. Deposita* 39, 344–357.
- Cooke, D.R., Bull, S.W., Large, R.R., McGoldrick, P.J., 2000. The importance of oxidized brines for the formation of Australian Proterozoic stratiform sediment-hosted Pb–Zn (Sedex) deposits. *Econ. Geol.* 95, 1–18.
- Cook, N.J., Ciobanu, C.L., Pring, A., Skinner, W., Shimizu, M., Danyushevsky, L., Sainieidukat, B., Melcher, F., 2009. Trace and minor elements in sphalerite: a LAICPMS study. *Geochim. Cosmochim. Acta* 73, 4761–4791.
- Davis, D.W., Lowenstein, T.K., Spencer, R.J., 1990. Melting behavior of fluid inclusions in laboratory grown halite crystals in the systems NaCl–H₂O, NaCl–KCl–H₂O, NaCl–MgCl₂–H₂O and NaCl–CaCl₂–H₂O. *Geochim. Cosmochim. Acta* 54, 591–601.
- Delouie, E., Turcotte, D., 1989. The flow of hot brines in cracks and the formation of ore deposit. *Econ. Geol.* 84, 2217–2225.
- Di Benedetto, F., Bernardini, G.P., Costagliola, P., Plant, D., Vaughan, D.J., 2005. Compositional zoning in sphalerite crystals. *Am. Mineral.* 90, 1384–1392.
- Dill, H.G., Sachsenhofer, R.F., Grecula, P., Sasvari, T., Palinkaš, L.A., Borojević-Šoštarić, S., Strmic-Palinkas, S., Prochaska, W., Garuti, G., Zaccarini, F., Arbouille, D., Schulz, H.M., 2008. Fossil fuels, ore and industrial minerals. In: McCann, T. (Ed.), *Geology of Central Europe*. Geological Society of London, Special Publication, London.
- Dill, H.G., 2010. Diagenetic and epigenetic mineralization in Central Europe related to surfaces and depositional systems of sequence stratigraphic relevance. In: Ketzer, M., Morad, S., De Ros, L.F. (Eds.), *Linking Diagenesis to Sequence Stratigraphy of Sedimentary Rocks*. International Association of Sedimentologists (IAS), Special Publication, Blackwell.
- Dill, H.G., Weiss, W., Botz, R., Dohrmann, R., 2011. Paleontological, mineralogical and chemical studies of syngenetic and epigenetic Pb–Zn–Ba–P mineralizations at the stratotype of the K/P boundary (El Kef area, Tunisia). *Int. J. Earth Sci.* 100, 805–846.
- Dubois, M., Marignac, C., 1997. The H₂O–NaCl–MgCl₂ ternary phase diagram with special application to fluid inclusion studies. *Econ. Geol.* 92, 114–119.
- Ehya, F., Lotfi, M.I., Rasa, I., 2010. Emarat carbonate-hosted Zn–Pb deposit, Markazi Province, Iran: a geological, mineralogical, and isotopic (S, Pb) study. *J. Asian Earth Sci.* 37, 186–194.
- Förster, H., 1974. Magmentypen und Erzlagertstätten im Iran. *Geol. Rundsch.* 63, 276–292.
- Förster, H., 1978. Mesozoic-Cenozoic metallogenesis in Iran, Part 4. *J. Geol. Soc. London* 135, 443–456.
- Ghasemi, A., Talbot, C.J., 2006. A new tectonic scenario for the Sanandaj-Sirjan Zone (Iran). *J. Asian Earth Sci.* 26, 683–693.
- Ghazban, F., McNutt, H., Schwarcz, H.P., 1994. Genesis of sediment-hosted Zn–Pb–Ba deposits in the Irankuh district, Esfahan area, west-central Iran. *Econ. Geol.* 89, 1262–1278.
- Ghorbani, M., 2013. *The Economic Geology of Iran, Mineral Deposits and Natural Resources*. Springer.
- Gilg, H.A., Boni, M., Balassone, G., Allen, C.R., Banks, D., Moore, F., 2006. Marble-hosted sulfide ores in the Angouran Zn–(Pb–Ag) deposit, NW Iran: interaction of sedimentary brines with a metamorphic core complex. *Miner. Deposita* 41, 1–16.
- Giordano, T.H., 2000. Organic matter as transport agent in ore-forming systems. *Econ. Geol.* 9, 133–156.
- Giordano, T.H., 2002. Transport of Pb and Zn by carboxylate complexes in basinal ore fluids and related petroleum-field brines at 100 °C: the influence of pH and oxygen fugacity. *Geochim. Trans.* 38, 56–72.
- Goldstein, R.H., Reynolds, T.J., 1994. Systematics of fluid inclusions in diagenetic minerals. *Soc. Econ. Geol. Paleontol.*
- Golonka, J., 2004. Plate tectonic evolution of the southern margin of Eurasia in the Mesozoic and Cenozoic. *Tectonophysics* 381, 235–273.
- Gustafson, L.B., Williams, N., 1981. Sediment hosted stratiform deposits of copper, lead, and zinc. *Econ. Geol.*, 75th Anniversary volume, 139–178.
- Hanor, J.S., 1994. Origin of saline fluids in sedimentary basins. In: Patnell, J. (Ed.), *Geofluids: Origin and Migration of Fluids in Sedimentary Basins*. Geological Society of London.
- Hanor, J.S., 1996. Controls on the solubilization of lead and zinc in basinal brines. In: Sangster, D.F. (Ed.), *Carbonate-Hosted Lead-Zinc Deposits*. SEG Special Publications.
- Hanor, J.S., 2001. Reactive transport involving rock buffered fluids of varying salinity. *Geochim. Cosmochim. Acta* 65, 3721–3732.
- Hitchon, B., Friedman, I., 1969. Geochemistry and origin of formation waters in the western Canada sedimentary basin: I. Stable isotopes of hydrogen and oxygen. *Geochim. Cosmochim. Acta* 33, 1321–1349.
- Hitzman, M.W., 1999. Extensional Faults that Localized Syndiagenetic Zn–Pb Deposits and Their Reactivation During Variscan Compression. Geological Society of London Special Publication.
- Hitzman, M.W., Beaty, D.W., 1996. *The Irish Zn–Pb–(Ba) Ore Field*. Society of Economic Geologists Special Publication.
- Hosseini-Dinani, H., Aftabi, A., 2016. Vertical lithogeochemical halos and zoning vectors at Goushfil Zn–Pb deposit, Irankuh district, southwestern Isfahan, Iran: implications for concealed ore exploration and genetic models. *Ore Geol. Rev.* 72, 1004–1021.
- Hooper, R.J., Baron, L., Hatcher Jr., R.D., Agah, S., 1994. The development of the southern Tethyan margin in Iran after the break-up of Gondwana implications for the Zagros hydrocarbon province. *Geosci. Iran* 4, 72–85.
- Hudson, M.R., 2000. Coordinated strike-slip and normal faulting in the southern Ozark dome of northern Arkansas: deformation in a late Paleozoic foreland. *Geology* 28, 511–514.
- Jankovic, S., 1977. The copper deposits and geotectonic setting of the Tethyan Eurasian metallogenic belt. *Miner. Deposita* 12, 37–47.
- Jankovic, S., 1997. The Carpatho-Balkanides and adjacent area: a sector of the Tethyan Eurasian metallogenic belt. *Miner. Deposita* 32, 426–433.
- Jazi, M.A., Karimpour, M.H., Malekzadeh Shafaroudi, A., 2017. Nakhlak carbonate-hosted Pb(U)Ag deposit, Isfahan province, Iran: a geological, mineralogical, geochemical, fluid inclusion, and sulfur isotope study. *Ore Geol. Rev.* 80, 27–47.
- Kramer, V., Hirth, H., Hofherr, W., Trah, H.P., 1987. Phase studies in the systems Ag₂Te–Ga₂Te₃, ZnSe–In₂Se₃, and ZnS–Ga₂S₃. *Thermochim. Acta* 112, 89–94.
- Kesler, S.E., Martini, A.M., Appold, M.S., Walter, L.M., Huston, T.J., Furman, F.C., 1996. Na–Cl–Br systematics of fluid inclusions from Mississippi Valley-type deposits, Appalachian Basin: constraints on solute origin and migration paths. *Geochim. Cosmochim. Acta* 60, 225–233.
- Kesler, S.E., 2005. Ore forming solutions. *Elements* 1, 13–18.
- Keyser, K., Hiatt, E.E., 2003. Fluids in sedimentary basins: an introduction. *J. Geochem. Explor.* 80, 139–149.
- Kharaka, Y.K., Maest, A.S., Carothers, W.W., Law, L.M., Lamothe, P.J., Fries, T.L., 1987. Geochemistry of metal-rich brines from central Mississippi Salt Dome basin, U.S.A. *Appl. Geochem.* 2, 541–560.
- Kharaka, Y.K., Carothers, W.W., 1986. Oxygen and hydrogen isotope geochemistry of deep basin brines. Chapter 2 In: Fritz, P., Fontes, J.Ch. (Eds.), *Handbook of Environmental Isotope Geochemistry*. Elsevier, pp. 305–360.
- Kharaka, Y.K., Hanor, J.S., 2007. Deep fluids in the continents: I. Sedimentary basins. In: Drever, J.I. (Ed.), *Surface and Ground Water. Weathering and Soils. Treatise on Geochemistry*, pp. 1–48.
- Kibitlewski, S., 1991. Tectonic control of the origin of the Zn–Pb deposits in the Chrzanow region, Poland. *Geol. Q.* 37, 229–240.
- Kucha, H., Schroll, E., Raith, J.G., Halas, A., 2010. Microbial sphalerite formation in carbonate-hosted Zn–Pb Ores, Bleiberg, Austria: micro- to nanotextural and sulfur isotope evidence. *Econ. Geol.* 105, 1005–1023.
- Leach, D.L., Sangster, D.F., 1993. Mississippi Valley-type lead-zinc deposits. *Geol. Assoc. Canada* 40, 289–314.
- Leach, D.L., Sangster, D.F., Kelley, K.D., Large, R.R., Garven, G., Allen, C.R., Gutzmer, J., Walters, S., 2005. Sediment-hosted lead–zinc deposits: a global perspective. *Econ. Geol.*, 100th Anniversary volume, 561–608.
- Leach, D., Macquar, J.-C., Lagneau, V., Leventhal, J., Emsbo, P., Premo, W., 2006. Precipitation of lead-zinc ores in the Mississippi Valley-type deposit at Trèves, Cévennes region of Southern, France. *Geofluids* 6, 24–44.
- Lin, Y., Cook, N.J., Ciobanu, C.L., Liu, Y., Zhang, Q., Liu, T., Gao, W., Yang, Y., Danyushevskiy, L., 2011. Trace and minor elements in sphalerite from base metal deposits in South China: A LA-ICPMS study. *Ore Geol. Rev.* 39, 188–217.
- Lisenbee, A.L., Uzunlar, N., 1988. Pb–Zn mineralization at Anjireh-Vejin mines, Sanandaj-Sirjan zone, Iran. In: Kisvarsanyi, G., Grant, S.K., Pratt, W.P., Koenig, J.W. (Eds.), *Proceedings Volume of the International Conference on Mississippi Valley type Lead-zinc Deposits*. University of Missouri-Rolla, Missouri, pp. 180–187.
- Lockington, J.A., Cook, N.J., Ciobanu, C.L., 2014. Trace and minor elements in sphalerite from metamorphosed sulphide deposits. *Mineral. Petrol.* 108, 873–890.
- Machel, H.G., 2001. Bacterial and thermochemical sulfate reduction in diagenetic settings; old and new insights. *Sed. Geol.* 140, 143–175.
- McQuarrie, N., Stock, J.M., Verdel, C., Wernick, B.P., 2003. Cenozoic evolution of Neo-Tethys for the causes of plate motions. *Geophys. Res. Lett.* 30, 4p.
- Mohajjel, M., Fergusson, C.L., 2000. Dextral transpression in Late Cretaceous continental collision, Sanandaj-Sirjan zone, western Iran. *J. Struct. Geol.* 22, 1125–1139.
- Mohajjel, M., Fergusson, C.L., Sahandoi, M.R., 2003. Cretaceous-Tertiary convergence and continental collision, Sanandaj-Sirjan zone, western Iran. *J. Asian Earth Sci.* 21, 397–412.
- Momenzadeh, M., Rastad, E., 1973. Zinc, Lead and Iron Mineralization in Cretaceous Crabonatic Rocks in the West-Central Iran Metallogenic Zone. Geological Survey of Iran In Farsi.
- Momenzadeh, M., 1976. In: *Stratabound Lead-Zinc Ores in the Lower Cretaceous and Jurassic Sediments in the Malayer–Esfahan District (West Central Iran)*, Lithology, Metal Content, Zonation and Genesis [Unpublished Ph.D. thesis]. University of Heidelberg, Heidelberg, West Germany, pp. 300.
- Momenzadeh, M., Shafighi, S., Rastad, E., Amstutz, G.S., 1979. The Ahangan lead-silver

- deposit, Se-Malayer, west Central Iran. *Miner. Deposita* 14, 323–341.
- Moritz, R., Ghazban, F., Singer, B., 2006. Eocene gold ore formation at Muteh, Sanandaj-Sirjan Tectonic Zone, Western Iran: a result of late-stage extension and exhumation of metamorphic basement rocks within the Zagros Orogen. *Econ. Geol.* 101, 1497–1524.
- Nabatian, G.H., Rastad, E., Neubauer, F., Honarmand, M., Ghaderi, M., 2015. Iron and Fe–Mn mineralisation in Iran: implications for Tethyan metallogeny. *Aust. J. Earth Sci.* 62, 211–241.
- Nejadhadad, M., Taghipour, B., Zarasvandi, A., Karimzadeh Somarin, A., 2016. Geological, geochemical, and fluid inclusion evidences for the origin of the Ravanj Pb–Ba–Ag deposit, north of Delijan city, Markazi Province, Iran. *Turk. J. Earth Sci.* 24, 1501–1526.
- Ohmoto, H., Rye, R.O., 1979. Isotopes of sulfur and carbon. In: Barnes, H.L. (Ed.), *Geochemistry of Hydrothermal Ore Deposits*. Wiley Interscience, New York.
- Ohmoto, H., Goldhaber, M.B., 1997. Sulfur and carbon isotopes. In: Barnes, H.L. (Ed.), *Geochemistry of Hydrothermal Ore Deposits*, third ed. John Wiley and Sons, New York, pp. 517–611.
- Person, M.A., Garven, G., 1994. A sensitivity study of the driving forces on fluid flow during continental rift evolution. *Geol. Soc. Am. Bull.* 106, 461–475.
- Peever, J., Fayek, F., Misra, K.C., Riciputi, L.R., 2003. Sulfur isotope microanalysis of sphalerite by SIMS: constraints on the genesis of Mississippi valley-type mineralization, from the Mascot-Jefferson City district, East Tennessee. *J. Geochem. Explor.* 80, 277–296.
- Phillips, G.N., Evans, K.A., 2004. Role of CO₂ in the formation of gold deposits. *Nature* 429, 860–863.
- Plumlee, C.S., Leach, D.L., Hofstra, A.H., Landis, G.P., Rowan, E.L., Viets, J.C., 1994. Chemical reaction path modeling of ore deposition in Mississippi Valley type Pb–Zn deposits of the Ozark region, U.S. midcontinent. *Econ. Geol.* 89, 1361–1383.
- Rajabi, A., Rastad, E., Canet, C., 2012. Metallogeny of Cretaceous carbonate-hosted Zn–Pb deposits of Iran: geotectonic setting and data integration for future mineral exploration. *Int. Geol. Rev.* 56, 1–24.
- Rastad, E., Fontbote, L., Amstutz, G.C., 1980. Relation between tidal flat facies and diagenetic ore fabrics in the strataband Pb–Zn–(Ba–Cu) deposits of Irankuh, Esfahan, West Central-Iran. *Rev. Inst. Invest. Geol. Diputacion Provin. Univ. Barcelona* 34, 311–323.
- Rittenhouse, G., 1967. Bromine in oil-field waters and its use in determining possibilities of origin of these waters. *Am. Assoc. Petrol. Geol. Bull.* 51, 2430–2440.
- Roberts, S.J., Nunn, J.A., Cathles, L.M., Cipriani, F.D., 1996. Expulsion of abnormally pressured fluids along faults. *J. Geophys. Res.* 101, 28231–28252.
- Roedder, E., 1984. Fluid inclusions. In: Ribbe, R.H. (Ed.), *Reviews in Mineralogy*. Mineralogical Society of America, pp. 646.
- Rowan, E.L., Leach, D.L., 1989. Constraints from fluid inclusions on sulfide precipitation mechanisms and ore fluid migration in the Viburnum Trend lead district, Missouri. *Econ. Geol.* 84, 1948–1965.
- Rowan, E.L., Goldhaber, M.B., 1995. Duration of mineralization and fluid-flow history of the Upper Mississippi Valley zinc-lead district. *Geology* 23, 609–612.
- Sangster, D.F., 1990. Mississippi Valley type and SEDEX lead-zinc deposits: A comparative examination. *Trans. Inst. Min. Metall.* 99, 21–42.
- Seal II, R.R., 2006. Sulfur isotope geochemistry of sulfide minerals. *Rev. Mineral. Geochem.* 61, 633–677.
- Seton, M., Müller, R.D., Zahirovic, S., Gaina, C., Torsvik, T., Shephard, G., Talsma, A., Gurnis, M., Turner, M., Maus, S., Chandler, M., 2012. Global continental and ocean basin reconstructions since 200 Ma. *Earth Sci. Rev.* 113, 212–270.
- Seyed Emami, K., Brants, A., Bozorgnia, F., 1973. Stratigraphy of the Cretaceous rocks. SE of Esfahan. Contribution to the Paleontology Stratigraphy of Iran. *Iran Geol. Surv. Deputy* 20 (Pt. 2), 5–27.
- Shadlun, T.N., 1982. Ore textures as indicators of formation conditions of mineral paragenesis in different type of stratiform lead-zinc deposits. In: Amstutz, G.C., Goresy, A.E., Frenzel, G., Kluth, C., Moh, G., Wauschkuhn, A., Zimmermann, R.A. (Eds.), *Ore Genesis-the State of the Art*. Springer, Heidelberg, pp. 607–624.
- Shelton, K.L., Gregg, J.M., Johnson, A.W., 2009. Replacement dolomites and ore sulfides as recorders of multiple fluids and fluid sources in the southeast Missouri Mississippi Valley-type district: Halogen-⁸⁷Sr/⁸⁶Sr-^δ18O-^δ34S systematic in the Bonnetterre Dolomite. *Econ. Geol.* 104, 733–748.
- Sicree, A.A., Barnes, H.L., 1996. Upper Mississippi Valley district ore fluid model: the role of organic complexes. *Ore Geol. Rev.* 2, 105–131.
- Sverjensky, D.A., 1984. Oil field brines as ore-forming solutions. *Econ. Geol.* 79, 23–37.
- Saunders, J.A., Swann, Ch.T., 1990. Trace-metal content of Mississippi oil field brines. *J. Geochem. Explor.* 37, 171–183.
- Scott, S.D., Barnes, H.L., 1971. Sphalerite geothermometry and geobarometry. *Econ. Geol.* 66, 653–669.
- Stöcklin, J., 1968. Structural history and tectonics of Iran: a review. *Am. Assoc. Pet. Geol. Bull.* 52, 1229–1258.
- Verdel, C., 2009. (I) Cenozoic Geology of Iran: An Integrated Study of Extensional Tectonics and Related Volcanism (II) Eadaicran Stratigraphy of the North American Cordillera: New Observation from Eastern California and Northern Utah. PhD thesis. California Institute of Technology, pp. 287.
- Verdel, C., Wernicke, B.P., Hassanzadeh, J., Guest, B., 2011. A Paleogene extensional flare-up in Iran. *Tectonics* 30, 20. <https://doi.org/10.1029/2010TC002809>.
- Verdel, C., 2013. The Eocene Golpaygan Metamorphic Core Complex, Central Iran: A Case History of Orogen-Parallel Forearc Rifting Along an Andean-type Contractional Margin. Tethyan Evolution and Seismotectonics of Southwest Asia. Honor of the 40 Years of Manuel Berberian's Research Contributions.
- Viets, J.G., Leach, D.L., 1990. Genetic implications regional and temporal trends in ore fluid geochemistry of Mississippi Valley-type deposits in Ozark region. *Econ. Geol.* 85, 842–861.
- Wight, D., Bradley, C., Leach, D., 2003. Tectonic controls of Mississippi Valley-type lead-zinc mineralization in orogenic forelands. *Miner. Deposita* 38, 652–667.
- Williams-Jones, A.E., Schrijver, K., Doig, R., Sangster, D.F., 1992. A model for epigenetic Ba–Pb–Zn mineralization in the Appalachian thrust belt: evidence from fluid inclusions and isotopes. *Econ. Geol.* 87, 154–174.
- Wilkinson, J.J., 2001. Fluid inclusions in hydrothermal ore deposit. *Lithos* 55, 229–272.
- Wilkinson, J.J., 2010. A review of fluid inclusion constraints on mineralization in the Irish Ore Field and implications for the genesis of sediment-hosted Zn–Pb deposits. *Econ. Geol.* 105, 417–442.
- Worden, R.H., Coleman, M.L., Matray, J.M., 1999. Basin scale evolution of formation waters; a diagenetic and formation water study of the Triassic Chaunoy Formation, Paris Basin. *Geochim. Cosmochim. Acta* 63, 2513–2528.
- Yardley, B.W.D., 2005. Metal concentrations in crustal fluids and their relationship to ore formation. *Econ. Geol.* 100, 613–632.
- Ziegler, K., Coleman, M.L., 2001. Palaeohydrodynamics of fluids in the Brent Group (Oseberg Field) (Brent Group, Norwegian North Sea) from chemical and isotopic compositions of formation waters. *Appl. Geochem.* 16, 609–632.
- Zahedi, M., 1975. Geological Map of Najafabad Quadrangle 6354. Geological Survey of Iran scale 1:100,000, 1 sheet.
- Zartman, R.E., Doe, B.R., 1981. Plumbotectonics the model. *Tectonophysics* 75, 135–162.
- Zisman, A., Momenzadeh, M., 1972. Study on Arak-Esfahan lead-zinc mines. *Geol. Surv. Iran* 60, 16.